運輸省港湾技術研究所

港湾技術研究所報告

REPORT OF
THE PORT AND HARBOUR RESEARCH INSTITUTE

MINISTRY OF TRANSPORT

VOL. 24 NO. 4 DEC. 1985

NAGASE, YOKOSUKA, JAPAN

港湾技術研究所報告 (REPORT OF P.H.R.I)

第24巻　第4号 (Vol. 24, No.4) 1985年12月 (Dec. 1985)

目　　次 (CONTENTS)

1. Field Observation of Local Sand Movements in the Surf Zone using Fluorescent Sand Tracer (Second Report)
..... Kazumasa KATOH, Norio TANAKA, Takamichi KONDOH, Masahiro AKAISHI and Kenji TERASAKI..... 3

(螢光砂を用いた砕波帯内における局所的砂移動の観測（第2報）
.....加藤一正・田中則男・近藤隆道・赤石正廣・寺崎賢次)

2. 波浪の統計的性質に関する二，三の数値的検討
.....合　田　良　実.....65

(Numerical Examination of Several Statistical Parameters of Sea Waves.....Yoshimi GODA)

REPORT OF THE PORT AND
HARBOUR RESEARCH INSTITUTE
Vol.24, No.4 (Dec. 1985)

1. Field Observation of Local Sand Movements in the Surf Zone using Fluorescent Sand Tracer (Second Report)

Kazumasa KATOH*
Norio TANAKA**
Takamichi KONDOH***
Masahiro AKAISHI***
Kenji TERASAKI****

Synopsis

Measurements of local sand movements in the surf zone have been carried out by using the fluorescent sand tracer on three beaches facing to the Pacific Ocean. The observation procedure employed in the field is as follows. The fluorescent sand tracers are injected in a point in the surf zone. Core samples are taken from sixteen points on a circumference of about 9 to 10 meters in radius around it with the time intervals of fifteen minutes for about five hours. Two horizontal components of current velocities are measured at the injection point by using an electromagnetic currentmeter. Based on the data of the particles numbers of sand tracer found in the core samples, the advection speed and its direction and the mixing depth of the fluorescent sand tracer have been analyzed to be related with the characteristics of waves and currents. The conclusions obtained in this report are as follows :

(1) The values of skewness for the incident wave components are positive, while those for the long-period one are negative, which make the values of skewness for the velocities combined of these two components to be negative.

(2) The advection speed of sand tracer in the mean current direction is 1% of the mean current velocity.

(3) The advection speed of sand tracer in the principal wave direction depends on not only the up-and-down asymmetry but also the before-and-behind asymmetry in the velocity profiles. The former asymmetry is considered to be related to the bed load transport and the latter one to the suspended load transport.

(4) The local mixing depth of the bed material is approximately proportional to the mean-square value of fluid velocities.

(5) For the first approximation, the set of equations for the local sand transport rate is proposed.

(6) The transporting conditions of suspended load are inferred so that the bed material may be intermittently transported in suspension in relatively short durations and be buried in the sea bottom due to the process of mixing of bed material during the remaining periods.

(7) The ratio of the absolute suspended load transport to the sum of the absolute transports of the suspended and the bed load becomes large with increase in the mean-square values of fluid velocities, which suggests that the suspended load transport will become to be more significant under the high wave conditions.

* Chief of Storm Surge and Tsunami Laboratory, Hydraulic Engineering Division
** Director of Marine Hydrodynamics Division
*** Former member of Littoral Drift Laboratory, Hydraulic Engineering Division
**** Member of Littoral Drift Laboratory, Hydraulic Engineering Division

港湾技術研究所報告
第24巻第4号（1985. 12）

1. 螢光砂を用いた砕波帯内における局所的砂移動の観測（第2報）

加藤一正*
田中則男**
近藤隆道***
赤石正廣***
寺崎賢次****

要　旨

螢光砂を用いて砕波帯内の局所的な砂移動の測定を，阿字ヶ浦海岸（1980年），大洗海岸（1981年），須田浜（1982年，1983年）において実施した。観測の方法は，砕波帯内の一点に螢光砂を投入し，投入点を中心にした半径約9～10mの円周上の16地点で，底質のコアサンプルを15分間隔で約5時間連続採取するものである。コアサンプル内の螢光砂を，暗室でカウントし，そのカウント数の経時変化および鉛直分布から，螢光砂の平均移動速度，混合深さを計算した。得られた結果は，同時に螢光砂投入点で電磁流速計によって測定した水平二成分の流速の代表値と関係付けた。

本調査ならびに解析で得られた結論は次のとおりである。

1) 波の主方向の流速成分の skewness が負になることがある。これは，その中に含まれる周期80～100 s程度の長周期波成分の skewness が負になっている影響が強く現れたためである。
2) 平均流方向への螢光砂の移動速度は，平均流の約1％である。
3) 入射波の主方向への螢光砂の移動は，流速波形の上下の非対称性だけではなく，前後の非対称性の影響を受ける。ここで，前後の非対称性の程度は加速度波形の skewness で評価した。
4) 螢光砂の混合深さは，その地点の流速変動の2乗平均値に比例する。
5) 螢光砂の移動速度と混合深さより局所的漂砂量式を求めた。
6) 砕波帯内における砂粒子の浮遊状態での移動は，間けつ的であり，移動していないときは海底面下に埋没していると推察された。
7) 砕波帯内の砂移動の形態は，流速変動の2乗平均値が増加するにつれて浮遊砂が相対的に卓越するようになる。

* 水工部　高潮津波研究室長
** 海洋水理部長
*** 前水工部　漂砂研究室
**** 水工部　漂砂研究室

Contents

Synopsis 3

1. **Introduction** 9

2. **Field Observations** 10
   - 2.1 Observation Procedure 10
   - 2.2 Sites of Field Observations 12
   - 2.3 General Conditions during Observations 16

3. **General Description of Sand Tracer Movements and Current Characteristics** 21
   - 3.1 Directional Distributions of Sand Tracer Movements 21
   - 3.2 Mixing Depth of Fluorescent Sand Tracer in the Sea Bottom 27
   - 3.3 Characteristics of Waves and Currents 32

4. **Relation between Movements of Fluorescent Sand Tracer and Fluid Dynamics** 42
   - 4.1 Advection Speed and Its Direction of Fluorescent Sand Tracer 42
   - 4.2 Coordinate System for Analyses 45
   - 4.3 Advection Speed of Sand Movement in the Direction of Mean Currents 47
   - 4.4 Advection Speed of Sand Movement in the Principal Wave Direction 50
   - 4.5 Mixing Depth of Sand Tracer 55
   - 4.6 Local Sand Transport Rate 58

5. **Summary** 60

References 61

Photo. 1 Taking of core samples by frog-men.

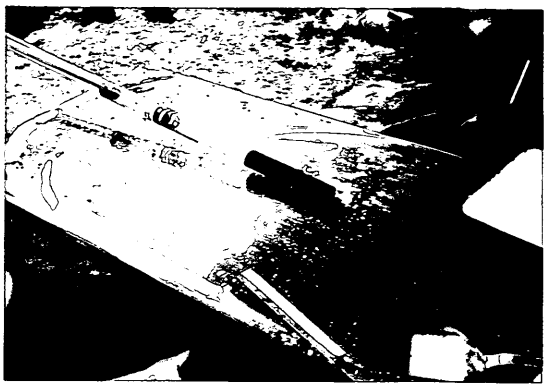

Photo. 2 Pushing out a core sample from the pipe.

Photo. 3 Core sample.

Photo. 4 Slicing the core sample into segments.

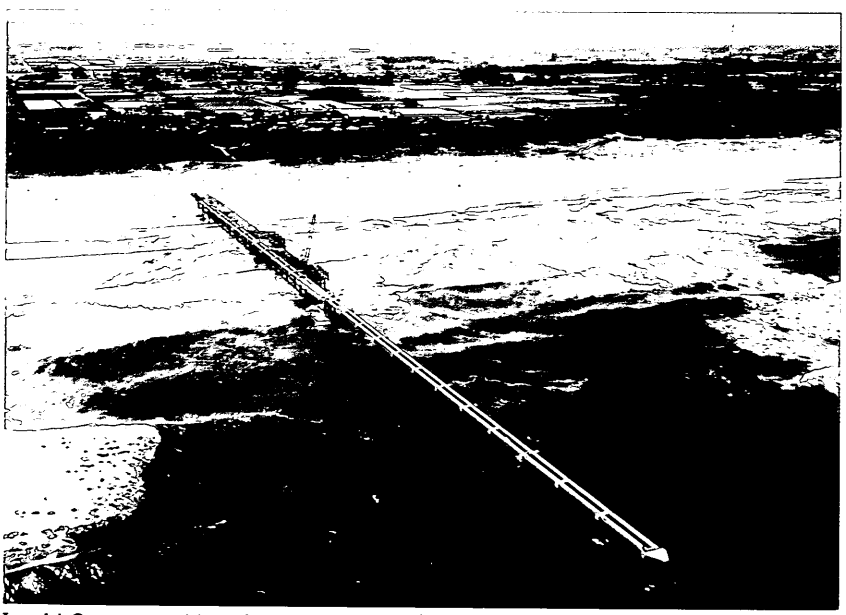

Photo. 5 Hazaki Oceanographical Research Facility (HORF), being under construction in September 1984.

1. Introduction

A region from the wave-breaking point to the shore is called the surf zone, in which a large amount of bed material is transported by the action of waves and their induced nearshore currents. Although our knowledge on the mechanics of sand movements in the surf zone have not been accumulated enough, we can easily see the results of it in the nearshore process, that is to say, the beach erosion and the sand accumulation.

It has passed more than a decade since an attempt to forecast the beach deformation by using electronic computers was begun. Up to the present day, a one-line-theory for computations has already been developed and improved to be put into practice. Some formula of longshore sand transport rate, which is the empirical relationship between the longshore component of wave energy flux carried into the surf zone and the resultant rate of longshore sand transport, is taken into this model. Since all of the phenomena in the surf zone are treated in a black box in the model, only the change of shoreline for a long period can be forecasted by using the one-line-theory.

There is also a necessity to predict the remaining beach processes such as the short term beach changes of several days during the storm wave conditions, the beach profile changes due to the onshore-offshore sand transport and three-dimensional changes of sea bottom configurations. The prediction becomes possible by the application of a three-dimensional model which are now under developing by many engineers and scientists. In the three-dimensional model, many phenomena in the surf zone should be treated in a transparent box. At present, the treatments of these phenomena can be divided into two parts. One is that for a calculation of the fluid dynamics of waves and currents. Another is that for a calculation of local sand transport rate and the resultant change of beach topography. The development of the former part seems to have been well progressing since its start, with the aid of a concept of the radiation stress. The latter one, however, is apt to be delayed because we have no reliable information about the local sand transport rate. Looking at the present state of the latter one, it might be said that the calculations in the former part, which are considered to be at a considerably high level, are no more than the manipulation, because we do not know enough what characteristics of fluid dynamics should be calculated for the local sand transport.

The study on the local sand transport in the surf zone is regarded as one of the very important themes in the coastal engineerings, and it is earnestly hoped to make clear the actual conditions of sediment dynamics in the surf zone. There is, however, a major obstacle to further understanding of the local sand transport, or nearshore sediment dynamics, that is to say, the lack of instruments which can directly measure the sediment transport.

In our first report (*Nadaoka*, *Tanaka* and *Katoh* 1981, which is referred to as "the first report" hereinafter), the authors developed the technique to use the fluorescent sand tracer for measuring the local sand movements in the surf zone, and examined its capability by applying it to the field, Ajigaura Beach in Japan. The result proved the technique quite promising, and we decided to explore its possibility further. The field observations with the fluorescent sand tracer have been carried on two beaches facing to the Pacific Ocean - Oarai Beach in 1981 and Sudahama Beach in 1982 and 1983, in Japan.

In this report, based on the data obtained by this method on these beaches, we examine the local sand movements such as the advection speed of sand tracer, the

mixing depth into the sea bottom, the sand transport rate, and so on.

2. Field Observations

2.1 Observation Procedure

An outline of the observation procedure employed in the field using fluorescent sand tracer is reviewed in this section. First of all, a circle with the radius R is established in the surf zone at an observation site as shown in Fig. 1. The radius R was 8.75 meters for almost all cases except one, in which it was 10 meters. In practice the circle is not drawn in the surf zone, but one pipe is set at the center of circle and sixteen pipes are set at the points which divide the circumference into sixteen arcs. The pipes are numbered clockwise from 1 to 16 so that a line passing through the pipes of No. 1 (offshore side) and No. 9 becomes normal to the shoreline. An electromagnetic current-meter is also set near the center of circle to measure the two horizontal components of the current velocity.

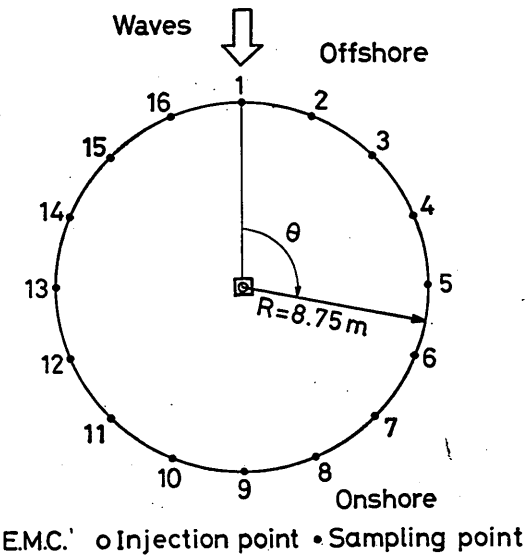

Fig. 1 Outline of observation procedure.

Three different colors of the fluorescent sand tracers, red, blue and yellow-green, are prepared in advance by utilizing the sand which have been previously removed from the beach face at the observation site. The observation starts at the time when one of the three colors of the tracers is injected at the center of circle. The remaining two colors of tracers are injected at the center at the time of one and two hours after the first injection, respectively. The volume of each sand tracer injected is 5 or 10 kilograms at a time. One of two methods of injection is used :

(a) A vinyl bag containing the tracer inside it is half buried in the sea bottom with its upper side being set at the same level as that of the sea bottom around. After that it is cut by a knife.

(b) A stainless steel container of 30 cm × 30cm × 4cm in size is half buried as the

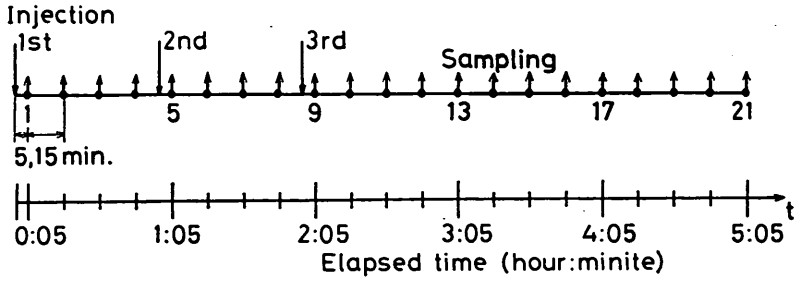

Fig. 2 Time table of the injections of the fluorescent sand tracer and the samplings.

same manner as the vinyl bag. In this case, however, the bottom plate is extracted slowly from the side and the container is pulled up smoothly leaving the fluorescent sand tracer in the sea bottom.

A sampling of the sand tracer at the sixteen points on the circumference is started 5 minutes after the first injection and is repeated with the time interval of 15 minutes, being 21 times for the typical case, as shown in Fig. 2. Therefore, the fifth and ninth samplings are performed at 5 minutes after the second and the third injections respectively.

Core samples are taken at all the sixteen points as shown in Fig. 3. The sampling procedure is as follows.

(a) A transparent acrylic pipe of about 130 centimeters in length, 3.4 centimeters in inner diameter and 3 milimeters in thickness is brought to the sampling point by a frogman.

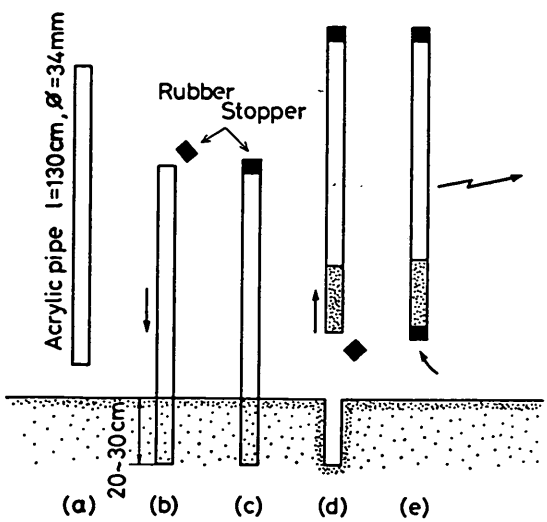

Fig 3. Method of taking core sample.

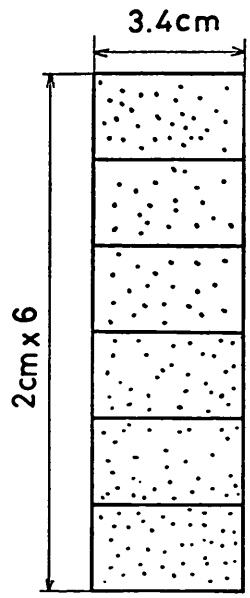

Fig. 4 Slice of core sample into segments.

(b) The acrylic pipe is pushed into the sea bottom by 20 to 30 centimeters.
(c) The upper end of pipe is sealed with a rubber stopper.
(d) The pipe is pulled out with the core sample inside it.
(e) Immediately after it, the lower end of pipe is sealed with another rubber stopper, and the pipe is brought to the shore. These works are done by eight frogmen, each man taking charge of two sampling points (see Photo. 1).

After removing the sea water, the core sample is slowly pushed out from the pipe onto a flat plate by using a piston, the diameter of which is only slightly smaller than the inner diameter of the pipe (see Photo. 2). In almost all cases, the core sample was able to be taken out in a cylindrical shape without being disturbed (see Photo. 3). The core sampe is then sliced into 2 centimeters segments from the sea bottom to the depth of 12 centimeters as shown in Fig. 4 (see Photo. 4), yielding 16 (points) $\times$ 21 (samplings) $\times$ 6 (segments) = 2016 segments per one typical experiment. These segments are carried to the laboratory. Each segment is well mixed, and about 40% of its quantity is spread out in the shape of a circular plate having the diamenter of 8 centimeters and the thickness of 0.15 centimeter on a flat plate in a pitch-dark room. Then, the number of the sand grains with each tracer color on the surface of the circular plate is counted ocularly under an ultraviolet light. Although the total number of tracer sand grains in one segment cannot be counted in this method, the number actually counted on the surface of fixed area is considered to be proportional to the total number.

2.2 Sites of Field Observations

The tracer experiments were carried out five times on three beaches on the east coast of Japan - Ajigaura (winter 1980, autumn 1980), Oarai (autumn 1981) and Sudaha-

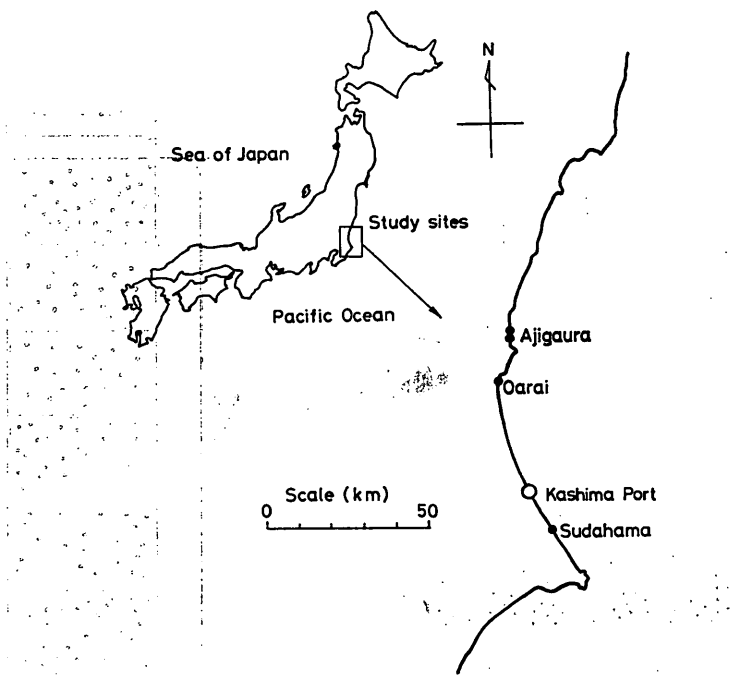

Fig. 5 Locations of study sites.

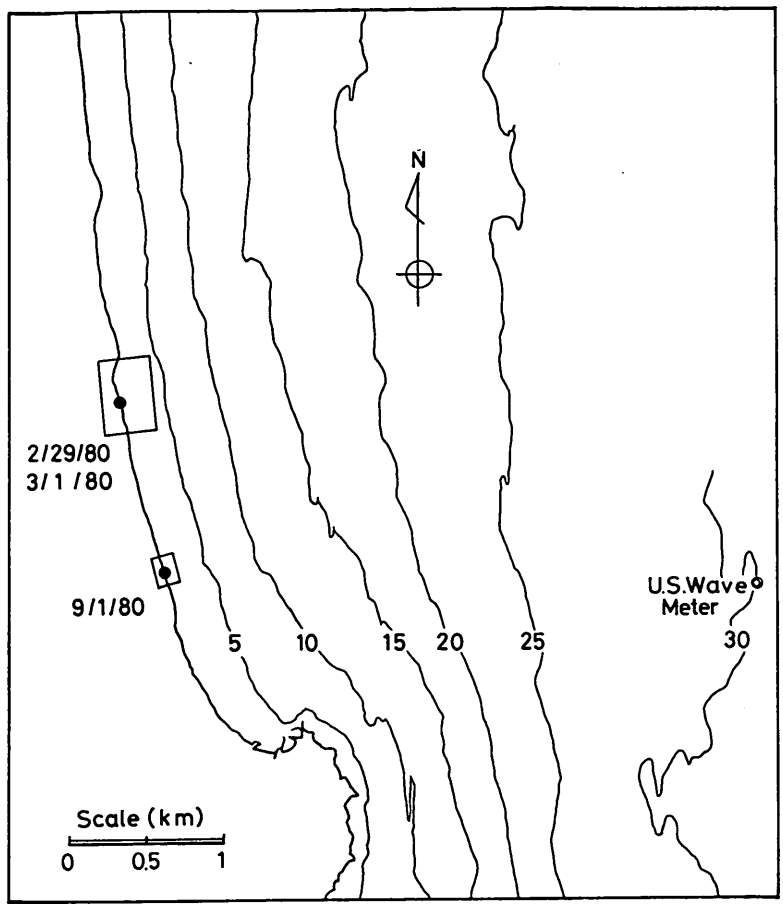

Fig. 6 Ajigaura Beach.

ma (summer 1982, summer 1983). These beaches are classified as micro-tidal beaches, because their tide ranges are about 1 meter. They are exposed to the full wave energy of the Pacific Ocean. The locations of these beaches are shown in Fig. 5, and the detailed topographies are shown in Fig. 6 (Ajigaura Beach), in Fig. 7 (Oarai Beach) and in Fig. 8 (Sudahama Beach).

An Outline of each beach will be described below.

[Ajigaura Beach]

Ajigaura Beach is located in the south side of an essentially straight coast of about 12 kilometers long. The south end of this coast is bounded by a cliff as shown in Fig. 6. On this beach is sited a sediment research pier of 200 meters long, built by the Public Works Research Institute, Ministry of Construction. Many researchers in Japan have observed nearshore phenomena on Ajigaura Beach by utilizing this facility, and have reported their results of studies (e.g., *Sasaki* and *Horikawa* 1975, 1978, *Hotta*, *Mizuguchi* and *Isobe* 1981, 1982, *Mizuguchi* 1982, *Hashimoto* and *Uda* 1982).

On this beach, the authors carried out the tracer experiments during the days of 29 February to 2 March 1980 and on 1 September 1980 and have reported in the first report [29], from which only the results of analyses will be quoted in this report.

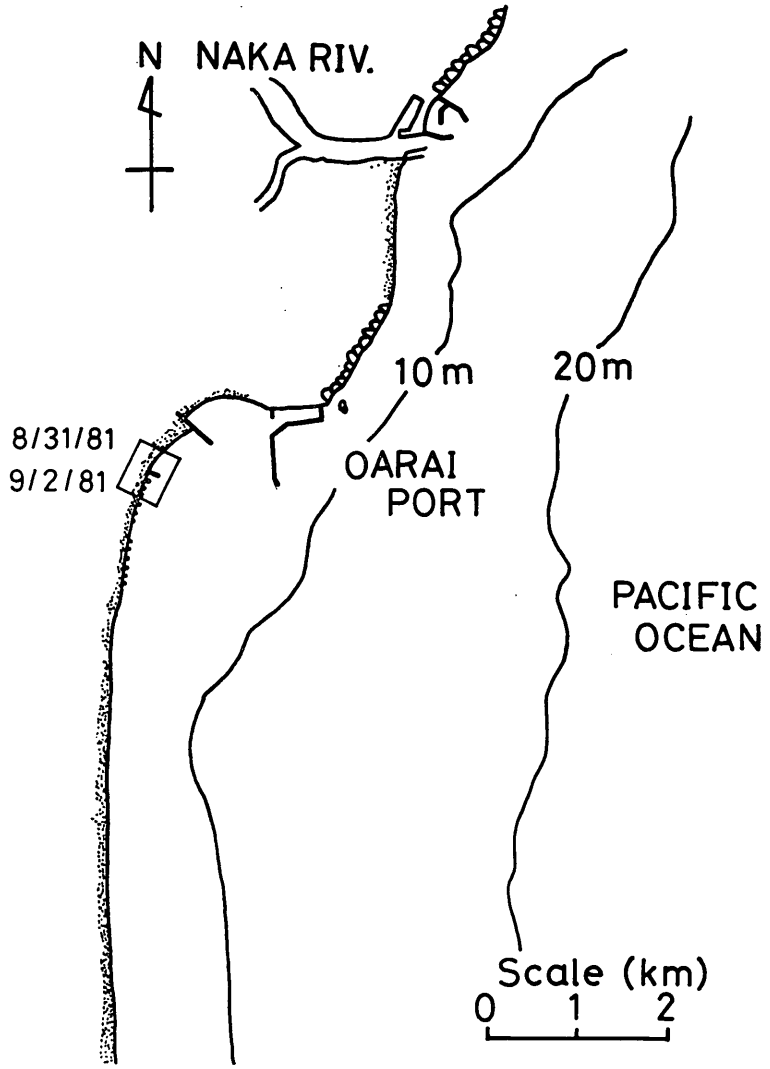

Fig. 7 Oarai Beach.

Further details of the field observations on this beach can be found in the first report.

[Oarai Beach]

Oarai Beach is located in the north end of a straight coast of Kashima of about 70 kilometers long, and is adjacent to Oarai Port (Fig. 7). Accompanying the prolongation of the breakwater of Oarai Port, the northward directional sand transport has become pronounced in the south-side beach. Therefore, in order to mitigate beach erosion and to prevent the sand from entering the anchorage, small groins in the eroded area and two jetties near the port have been constructed.

During last several years, the synthetic field observations on littoral drift were carried out in this beach to investigate the characteristics of waves and nearshore currents and the mechanics of sand transport in the surf zone, for the purpose of developing

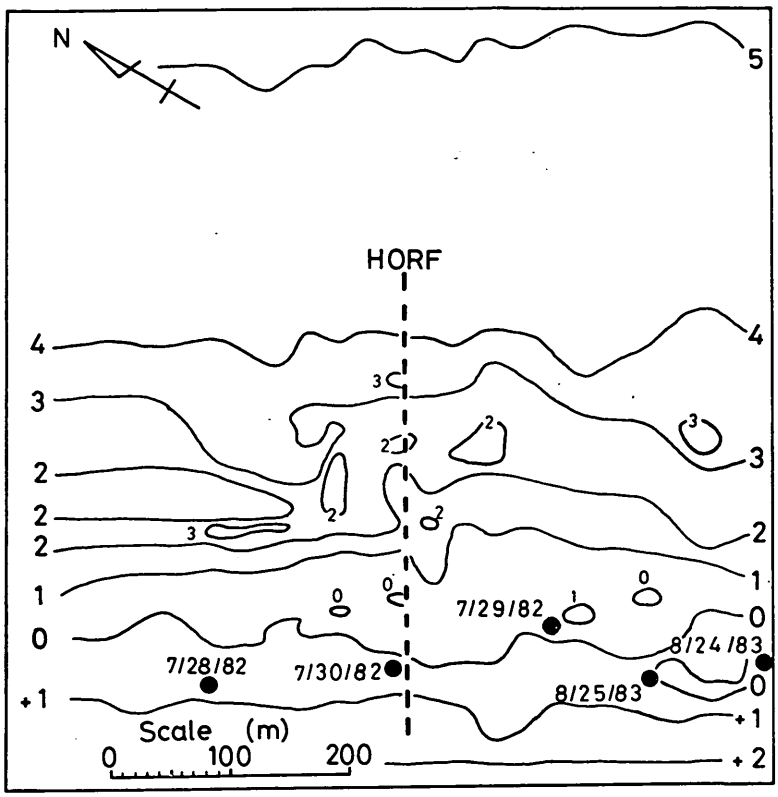

Fig. 8 Sudahama Beach.

numerical predictive models of the coastal process (e.g., *Hotta, Mizuguchi* and *Isobe* 1981, *Hattori* 1982, *Kraus, Hansen* and *Harikai* 1984, *Katoh, Tanaka* and *Irie* 1984, *Sunamura* and *Kraus* 1985, *Kraus* 1985).

The tracer experiments were carried out on 28 and 29 August 1982 at two points which were located about 300 meters north and south respectively from the smaller jetty (Fig. 9). These points were located inside the sheltered area from the incident waves by the breakwater of Oarai Port. Before the tracer experiments, the concentration of suspended load was measured in the surf zone on 26 and 27 August 1982. The result of data analysis on the suspended load can be found elsewhere (*Katoh, Tanaka* and *Irie* 1984).

[Sudahama Beach]

Sudahama Beach is located about 14 kilometers north from the south end of Kashima Coast. This beach is a entirely natural sandy beach without any artificial structures on the beach nor in the nearshore zone. However, the Hazaki Oceanographical Research Facility (HORF, a sediment research pier of 427 meters long) is being constructed since 1982 by the Port and Harbour Research Institute, Ministry of Transport, and it will be completed by the end of 1985 (Photo. 5). This beach is expected to function as a new theater of field observations on the nearshore environments.

The tracer experiments were carried out during the days of 28 to 30 July 1982, before the construction of the HORF, and on 24 and 25 August 1983, during its construction. In the latter case, observation points were selected about 200 to 250 meters

in the south of construction site. The observation site was located at the upstream side of longshore currents and no influence of the construction works was thought to be exerted on waves and currents.

In total the tracer experiments were carried out for eleven days. In this report, each experiment will be referred to by year, month and day ; that is to say, it will be numbered with the figures of month/day/year. For example, the experiment numbered by 7/30/82 means that it was carried out on July 30, 1982.

2.3 General Conditions during Observations

General conditions of the sea during the field observations are listed in Table 1. The seventh and the eighth columns of Table 1 give the mean values of significant wave heights and periods in deep water during the observations which have been measured at the depth of 30 meters below the datum line near Ajigaura Beach (see Fig. 6). The figures of wave height and period with the mark of "?" are the estimated values from the wave data immediately (about two hours) before the observation, because the wave measurements did not go well at the essential period. There were predominant long-period waves of about 80 to 100 seconds in periods in the current records obtained in the surf zone on Sudahama Beach in 1982 and 1983.

The ninth and tenth columns give the tidal levels at the times of start and end of the observations above the datum line which have been measured in Oarai Port (1980, 1981 and 1983) and in Kashima Port (1982) (see Figs. 5 and 7). The eleventh column gives the tide difference between the highest and the lowest tidal levels during the observations. An arrow in the twelfth column shows the rough trend of tidal level change. For example, the upward arrow means the rise of tidal level ; the horizontal arrow means that the tidal level was held nearly constant. The tide differences were the largest in 1983 on Sudahama Beach. Because of this, during the earlier stage of the low tide, the sensor of electromagnetic currentmeter occasionally emerged above the sea surface when the trough of waves passed through the measuring point. The emergence caused spike noises in the records of currents. Such data are not analyzed in the present study.

The last column of Table 1 gives the characteristics of the beach materials (quartz sand) at Ajigaura, Oarai and Sudahama beaches. The medium diameter of sand, d_{50}, is the value of the diamenter corresponding to the intersection of the 50th percentile on the cumulative grain size curve. The sorting coefficient S_o is defined as

$$S_o=(d_{75}/d_{25})^{1/2}, \tag{1}$$

and the skewness parameter S_k is defined as

$$S_k=(d_{75}\cdot d_{25})/d_{50}^2, \tag{2}$$

which indicates the degree of asymmetry of grain size distribution, where d_{25} and d_{75} are the values of diameters corresponding to the intersections of the 25th and 75th percentiles on the cumulative grain size curve.

The setup conditions of the electromagnetic currentmeter and representative characteristics of current velocities at the observation points (center of the circle) are listed in Table 2. The currentmeter is of two-component type, and measure two horizontal components of the current velocity.

A clearance listed in the third column in Table 2 is the vertical distance of the sensor of currentmeter from the sea bottom. As the sensor was held from the above,

Table 1 Summary of experiment conditions (part 1)

(1)	(2)	(3)	(4)	(5)	(6)	(7)	(8)	(9)	(10)	(11)	(12)	(13)
Site	Experiment Number	Start Time of Experiment	Amount of Tracer Injected ×Colors	Radius of Circle	Sampling times	$(H_{1/3})_0$ (m)	$(T_{1/3})_0$ (s)	Lowest Water Level (D.L.m)	Highest Water Level (D.L.m)	Tide Range (m)	General Trend of Water Level Change	Sediment Character-istics
Ajigaura Beach	2/29/80	10 : 34	20kg×1	10.00	8	0.70	8.2	0.63	0.85	0.22	↗	$d_{50}=0.22$mm
	3/ 1/80	9 : 40	10kg×1	10.00	9	0.71	6.5	0.64	0.93	0.29	↗	$S_o=1.12$
	3/ 2/80	9 : 10	10kg×1	10.00	9	1.12	8.9	0.61	0.62	0.10	→	$S_k=1.00$
	9/ 1/80	11 : 20	10kg×3	8.75	20	1.45	8.9	0.99	1.09	0.20	↗	
Oarai Beach	8/31/81	9 : 45	5kg×3	8.75	21	0.52	6.0	0.16	0.77	0.68	↗	$d_{50}=0.24$mm
	9/ 2/81	10 : 55	5kg×3	8.75	21	0.38	5.7	0.36	1.07	0.74	↗	$S_o=1.34$ $S_k=1.12$
Sudahama Beach	7/28/82	11 : 00	5kg×3	8.75	21	1.50	8.5	1.03	0.78	0.27	↘	$d_{50}=0.16$mm
	7/29/82	9 : 15	5kg×3	8.75	21	1.20	8.8	0.86	0.90	0.14	→	$S_o=1.17$
	7/30/82	9 : 30	5kg×3	8.75	21	1.00?	8.4?	0.75	1.00	0.25	↗	$S_k=0.99$
Sudahama Beach	8/24/83	11 : 00	5kg×3	8.75	21	1.02	5.7	0.26	1.31	1.05	↗	
	8/25/83	11 : 00	5kg×3	8.75	16	0.85	7.5	0.32	1.13	0.81	↗	

Table 2 Summary of experiment conditions (part 2)

(1)	(2)	(3)	(4)	(5)	(6)	(7)	(8)
Site	Experiment Number	Clearance (cm) (hour : minute)	Water Depth (cm) (hour : minute)	Mean Velocity (cm/s)	Velocity Skewness $\sqrt{\beta_1}$	long-crestedness γ^*	$\sqrt{\overline{U_p^2}}$ (cm/s)
Ajigaura Beach	2/29/80	10		8.0	0.37	0.69	25.7
	3/ 1/80	30		10.4	0.47	0.68	26.5
	3/ 2/80	13, 18		14.1	−0.01	0.52	32.6
	9/ 1/80			49.0	0.43	0.42	42.2
Oarai Beach	8/31/81	12(10 : 15), 15(15 : 00)		2.3	0.27	0.54	32.2
	9/ 2/81	8(11 : 00), 8(13 : 30)		27.5	0.72	0.40	28.9
Sudahama Beach	7/28/82	12(10 : 17), 20(12 : 30)	84(12 : 30), 76(15 : 40)	28.9	−0.27	0.47	42.0
	7/29/82	17(8 : 50), 25(14 : 40)	93(10 : 05), 98(11 : 40), 89(14 : 30)	60.2	0.15	0.51	43.2
	7/30/82	20(8 : 55)	70(10 : 20), 100(12 : 45)	55.4	−0.07	0.46	53.4
Sudahama Beach	8/24/83			16.0	0.19	0.55	34.0
	8/25/83	13(11 : 00), 17(12 : 00)		33.9	0.07	0.57	45.0

there was nothing but the sea water between the sensor and sea bottom. The clearance was measured by using a scale or a palm and fingers of a frogman, repeating twice in some cases. Because the latter measurement of the clearance usually showed a larger value, it is considered that the sea bottom was slightly eroded during the observation.

One more pipe was set outside the circle in 1982, to which a thin transparent tube was attached. The both ends of the tube were left open, and one end was in the air and another end was in the water. The water surface inside the tube moved up and down, amplitude of which, however, was very small compared with that of waves around the tube because of the dumping effect due to the viscous friction along the wall of tube. Therefore, the level of mean water surface could be roughly measured by

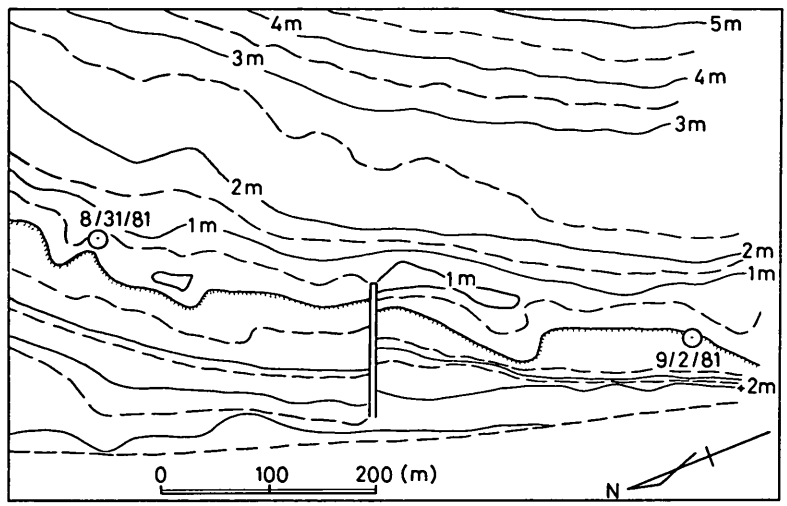

Fig. 9 Sampling points and beach topography on Oarai Beach (surveyed during 3 to 5 September 1981).

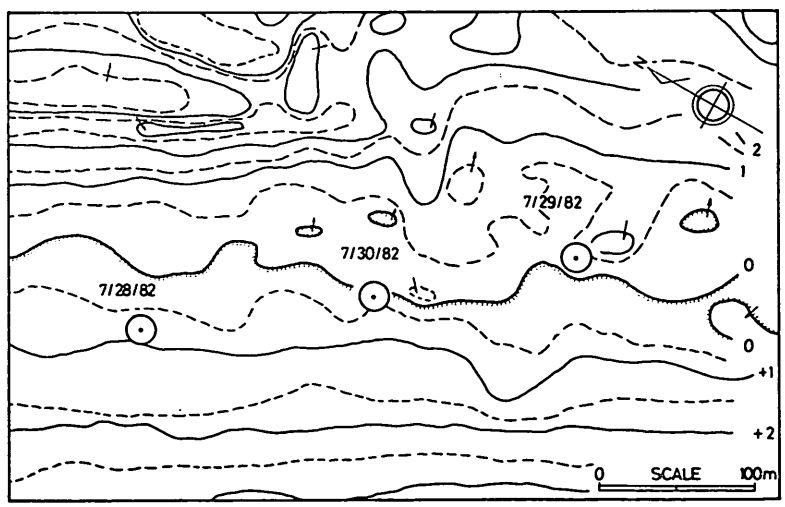

Fig.10 Sampling points and beach topography on Sudahama Beach (surveyed on 19 August 1982).

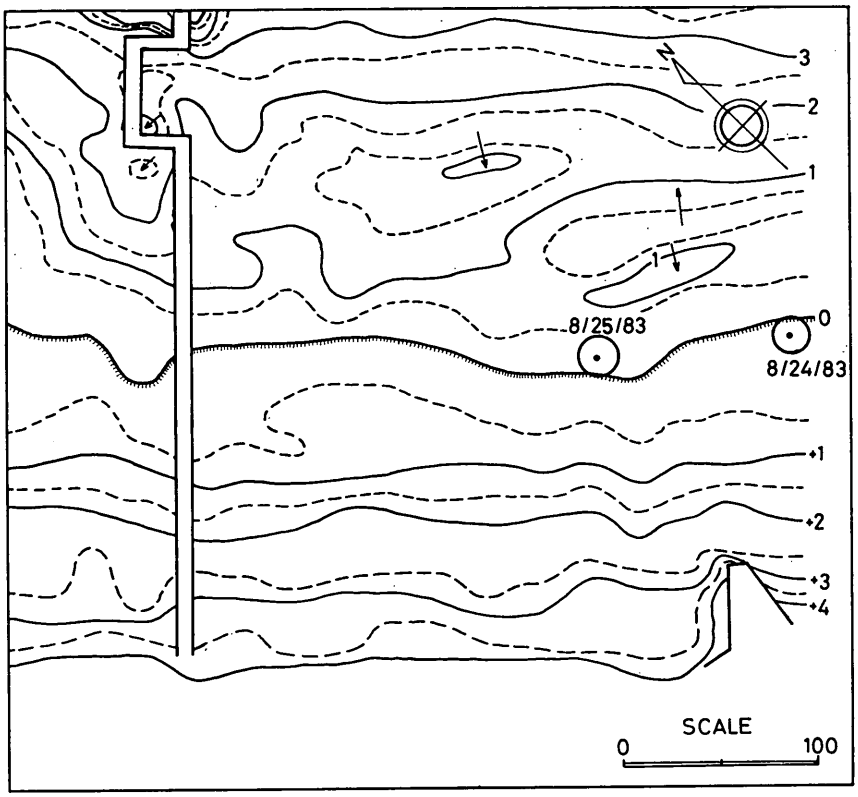

Fig.11 Sampling points and beach topography on Sudahama Beach (surveyed on 1 September 1983).

observing the mean position of water surface inside the tube. This works were done by the frogman. The results converted into the mean water depth are shown in the fourth column of Table 2. In other observations, the water depths were not measured, but they might be about one meter or less because the level of observation points were around the datum level (see Figs. 9, and 11), beyond which it became very difficult for the frogmen to take the core samples from the sea bottom in the surf zone.

The representative characteristics of currents and waves, that is to say, the mean velocity, the skewness, the long-crestedness and the root-mean-square values of velocities due to waves, are calculated by utilizing the two horizontal components of the current velocities and the resultant values are listed in Table 2. The calculation procedures will be explained in Section 3.3.

Figures 9, 10 and 11 show the sea bottom topographies around the observation points on Oarai Beach and Sudahama Beach. The observation of sand movements using fluorescent sand tracer was carried out at the ground elevation around the datum level, 0 meter, in both cases. This is because of the fact that we could not help deciding the locations of almost the same water depth for the sampling works by the frogmen. Because the water depths were not deep, the observation points were usually located inside the surf zone in all cases.

The topographies shown in Fig. 9, 10 and 11 are not those corresponding to the days when the observations were carried out. As seen in the dates of surveys shown in parentheses below the figures, there are lags of several days or more. Therefore there

may not be much points in examining the feature of topography in micoro-scale, because it would have been easily deformed by the action of waves and currents in the surf zone. One may have an impression that the sea bottom topography offshore-side of the observation points in 1982 (Fig. 10) was rather complicated one. In this area, however, the longshore interval (25 meters) of measurement lines for surveying was half of those of other area, because it was the site of HORF and the detailed survey data was needed before the construction. Then, the complication of topography may be due to dense data.

3. General Description of Sand Tracer Movements and Current Characteristics

In this chapter, a general description of sand tracer movements and current characteristics is made for the data obtained on Oarai Beach in 1981 and on Sudahama Beach in 1982 and 1983. Those on Ajigaura Beach in 1980 have been discussed in the first report [29].

3.1 Directional Distributions of Sand Tracer Movements

An outline of directional distributions of sand tracer movements is introduced for each case by utilizing the figures from Figs. 12 to 18. As these figures are prepared under the uniform style, a way of looking at them is explained at first.

In each figure, the figures on the ordinate of the left-hand side correspond to the sampling point numbers on the circumference (see Fig. 1), while those of the right-hand side correspond to the angle measured from the No. 1 point in the clockwise direction, respectively. The abscissa is the time which is the actual one on the lower-side and is the elapsed one from the first injection of fluorescent sand tracer on the upper-side. The vertical straight lines indicate the time when the core samples of bottom materials were taken at sixteen points on the circumference. The directional distributions of the total number of fluorescent sand tracer in the core sample with six segments (see Fig. 4) at each sampling time are shown with the solid lines, the broken lines and the dashdot lines for the tracers corresponding to the first, the second and the third injection, respectively. As the second injection of tracer was done at one hour after the

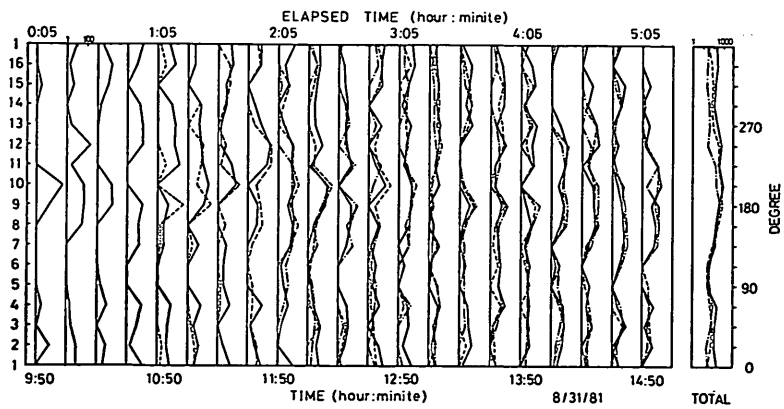

Fig.12 Directional distribuion of a number of fluorescsnt sand tracer on the circumference (8/31/81, Oarai Beach).

first injection, the broken lines for it are shown at the time on and after the elapsed time of 1 : 05. The dashdot lines for the third injection, two hours after the first one, are shown at the time on and after the elapsed time of 2 : 05. Note that the numbers of tracer are shown on a log scale, which is marked out on the abscissa in the upper-side. A long and slender figure adjacent to the right-hand side of main figure shows the distribution of total number of tracer in all core samples.
[8/31/81, Oarai Beach, Fig.12]

The tracers are distributed at all sampling points. This result corresponds to the feeble velocity of mean current (2.3cm/s on the average, see Table 2) and to the unsteadiness of the current direction (it gradually changed in the counterclockwise direction as shown in Fig.35).
[9/2/81, Oarai Beach, Fig.13]

All kinds of the tracer injected at the first, the second and the third times are distributed with a concentration to the sampling points of No.14 and No.15, displaying a bistinct direction of the tracer movements.
[7/28/82, Sudahama Beach, Fig.14]

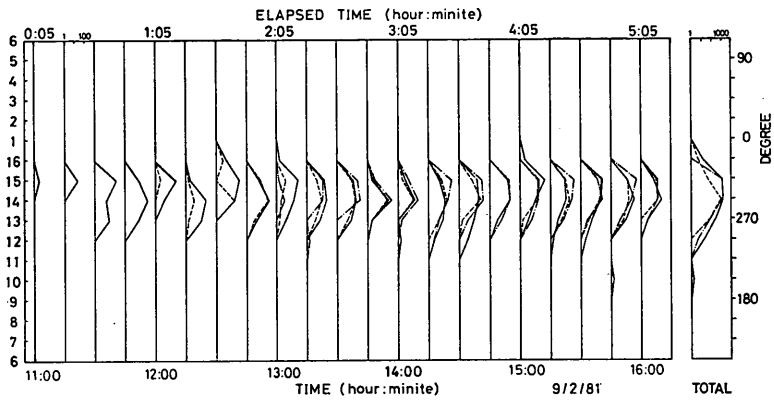

Fig.13 Directional distribution of a number of fluorescent sand tracer on the circumference (9/2/81, Oarai Beach).

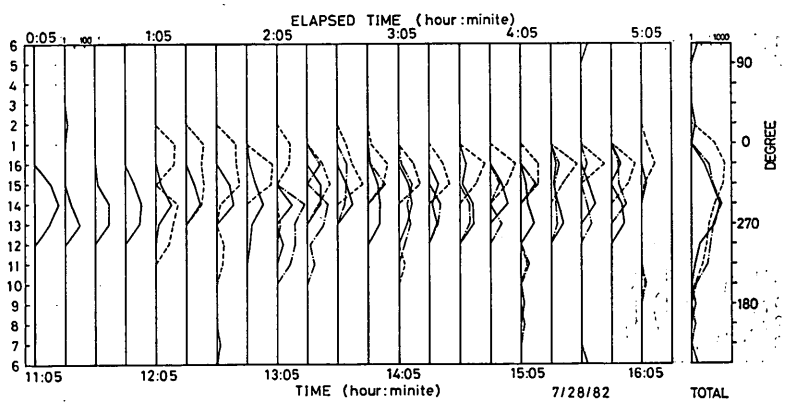

Fig.14 Directional distribution of a number of fluorescent sand tracer on the circumference (7/28/82, Sudahama Beach).

Also in this case, the directions of the tracer movements are almost fixed around the sampling point of No.15. The first and the third injected tracers are similarly distributed each other with peaks at the sampling point of No.14 in the total count numbers, while the second one shows the slightly different distribution with the peak at the sampling point of No 16.

[7/29/82, Sudahama Beach, Fig.15]

The count number of tracer is small at every sampling time. The number decreases quickly after the injection of each tracer, and only the third injected tracer is found in the latter half of measurements. This is because the injected tracers must have gone out fast from the circle due to the strongest mean current velocity of 60.2 cm/s on the average during the observation (see Table 2).

[7/30/82, Sudahama Beach, Fig.16]

Every kind of tracer is transported to the sampling point of No.14 in this case. Although the mean current velocity was very strong of 55.4 cm/s on the average (see Table 2), the count number of tracer is larger than that of case 7/29/82. This result is considered to be due to the fact that the mean current velocity was rather weaker in the first half, being unable to transport much of tracer outside the circle, but it became

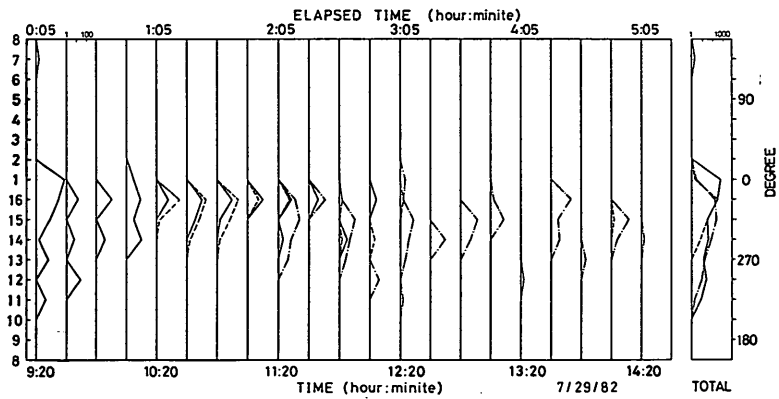

Fig.15 Directional distribution of a number of flurescent sand tracer on the circumference (7/29/82, Sudahama Beach).

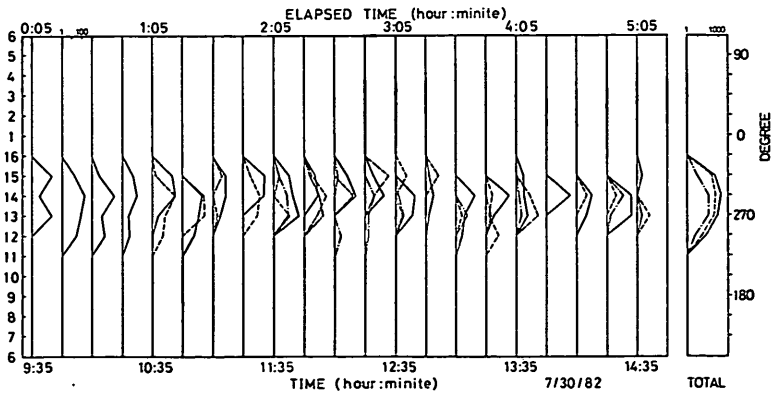

Fig.16 Directional distribution of a number of fluorescent sand tracer on the circumference (7/30/82, Sudahama Beach).

stronger in the latter half of observation period (see Fig.39).

[8/24/83, Sudahama Beach, Fig.17]

The direction of tracer movement gradually changes from the sampling point of No.12 at the elapsed time of about 1 : 05 to that of No.2 or 3 afterward. Therefore, the direction of total tracer movements is not so distinct with broad peaks among the sampling points of No.12 and No.2. The relationship between the changes of tracer movements and external forces of tracer transport, waves and currents, cannot be examined because the current data are not available (see Fig. 40) in the first half of the observation period as explained in Section 2.3. Only the third injected tracer will be analyzed further with the current data in Chapter 4.

[8/25/83, Sudahama Beach, Fig.18]

In this case, the work of taking the core samples was interrupted during the period of 12 : 30 to 13 : 30 in the the actual time by an accident that strong rip currents carried one of the frogmen toward the offshore, to whom the charge of sampling at the No.1 point was assigned. The third injection of the fluorescent sand tracer, however, was done at the time of two hours after the first injection as planned. In this observation, the experiment started at low tide when the notable rip currents did not exist

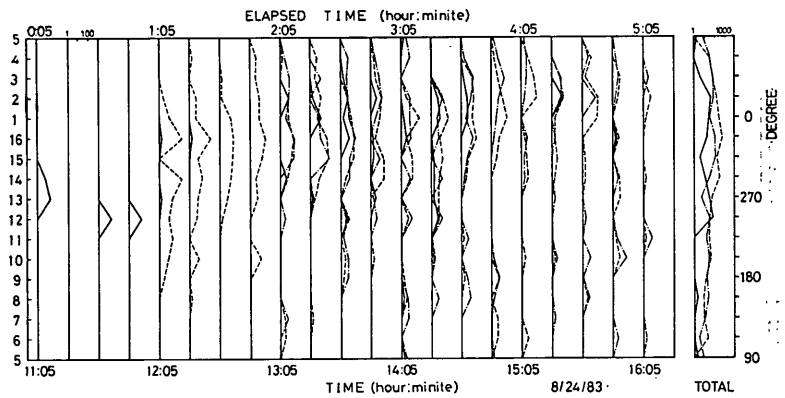

Fig.17 Directional distribution of a number of fluorescent sand tracer on the circumference (8/24/83, Sudahama Beach).

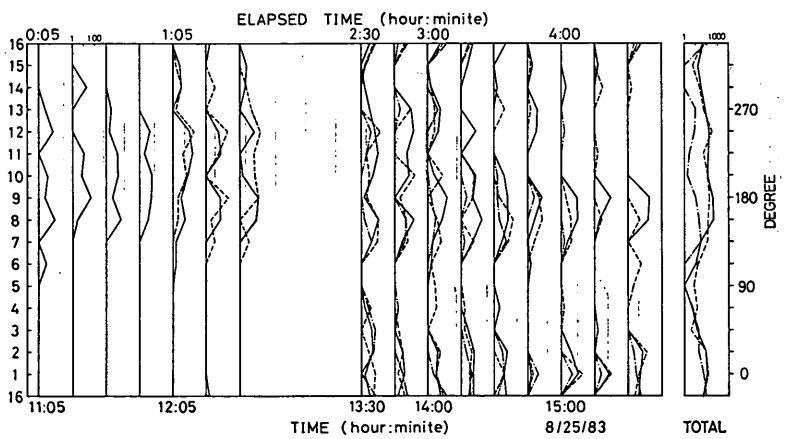

Fig.18 Directional distribution of a number of fluorescent sand tracer on the circumference (8/25/83, Sudahama Beach).

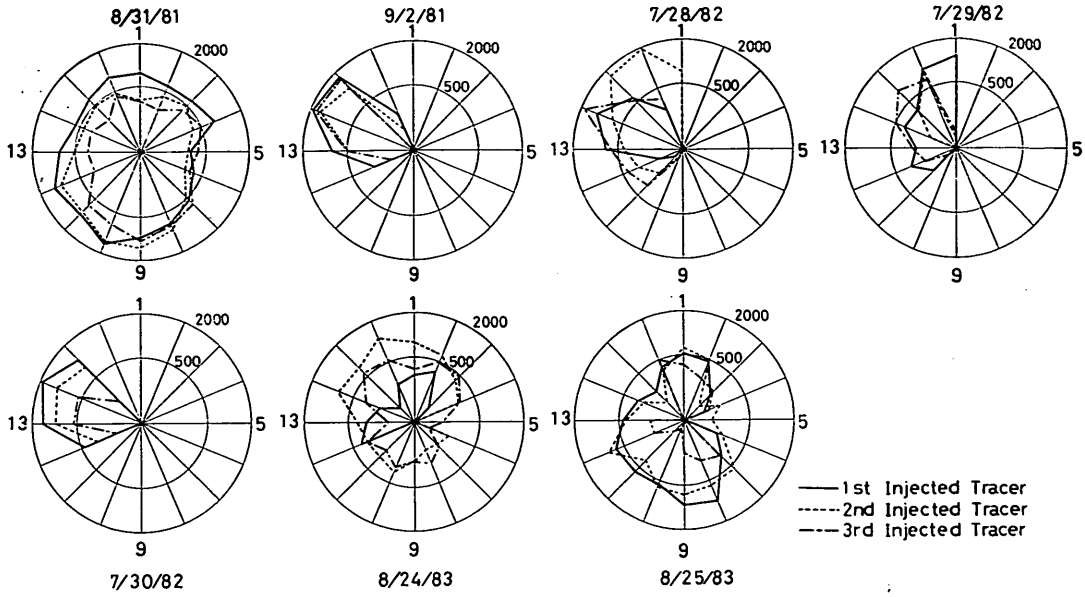

Fig.19 Spacial Distribution of tracer movements (total count number of tracer).

around the circle. The rip currents became stronger with time and with the rise of tidal levels. As can be seen in Fig.18, the sand tracer were transported to the sampling points between No.7 and No.14 before the accident, while they were also transported to the sampling point of No.1, in the offshore direction, after the accident. Like the previous case, the current data of this case at the center of circle have noises due to the emergence of the sensor of currentmeter above the sea surface in the first half of the observation period. Thus only the data of the third injected tracer will be analyzed further in Chapter 4.

The total count number of tracer shown on the right-hand in Fig.12 through Fig.18 are rearranged on circles in Fig.19 for easy understanding of the directional feature of tracer movements. Note again that the numbers of tracer are shown on a log scale, which is marked with a great circle of 2000 count and a small circle of 500 count.

Next, how the tracer scatted out from the circle is examined. For this purpose, the data of tracer number are rearranged to obtain the total number of tracer at every sampling time. Figure 20 through Fig.26 show their changes for each case, by plotting the total number on the ordinate and the time on the abscissa.

By comparing these figures, we can make the statement as follows :

(a) There are three trends of changes. The first is such that the count number is largeat first and decreases with time, the second is that it is small at first and increases with time, and the third is that there is no distinct changes of count number with time. The first trend can be recognized in the cases of 8/31/81, 7/28/82 and 8/24/83, while the second trend in the case of 9/2/81. The remaining cases of 7/30/82 and 8/25 /83 correspond to the third one.

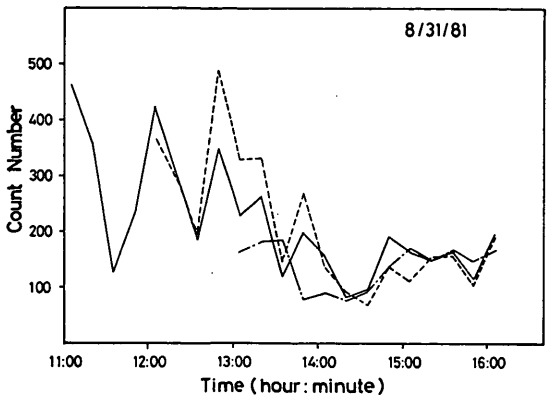

Fig.20 Change of the total count number of tracer with respect of time on the circumference (8/31/81, Oarai Beach).

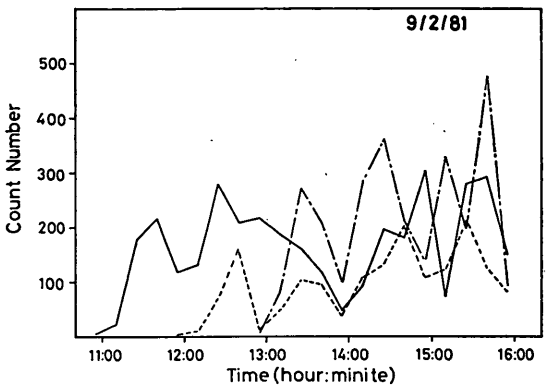

Fig.21 Change of the total count number of tracer with respect of time on the circumference (9/2/81, Oarai Beach).

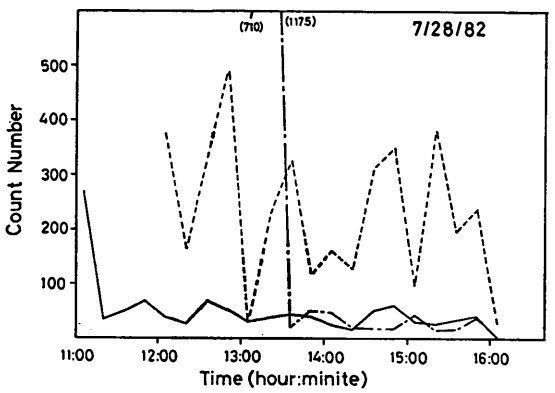

Fig.22 Change of the total count number of tracer with respect of time on the circumference (7/28/82, Sudahama Beach).

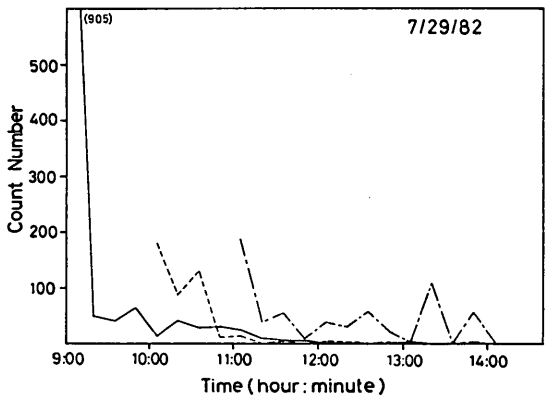

Fig.23 Change of the total count number of tracer with respect of time on the circmference (7/29/82, Sudahama Beach).

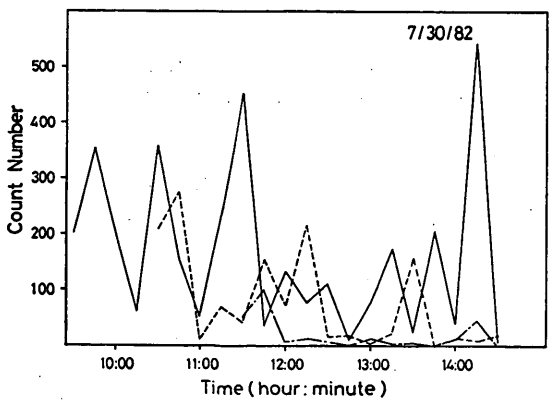

Fig.24 Change of the total count number of tracer with respect of time on the circumference (7/30/82, Sudahama Beach).

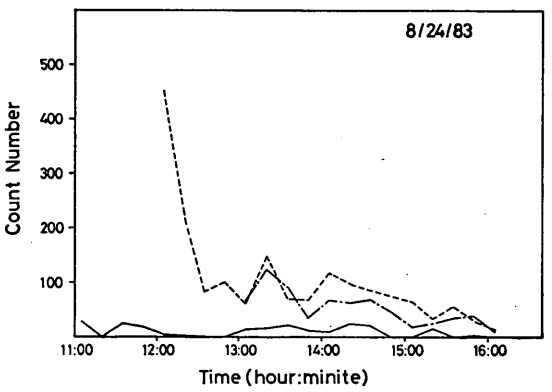

Fig.25 Change of the total count number of tracer with respect of time on the circumference (8/24/83, Sudahama Beach).

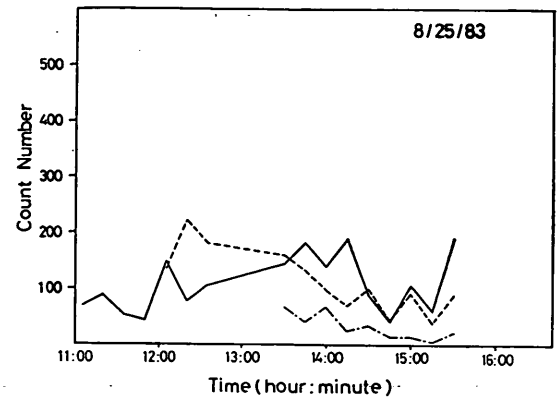

Fig.26 Change of the total count number of tracer with respect of time on the circumfercnee (8/25/83, Sudahama Beach).

(b) Although three kinds of tracer, being different in color, were injected at intervals of one hour, the count number changes similarly in some cases, that is, of 8/31/81, 9/2 /81 and 8/25/83.

(c) In the cases of 7/28/82, 7/29/82 and 8/24/83, there were time lags among three kinds of tracer in spite of the similarity of changes. In these cases, the count number is large at first, then quickly decreases, and stays at a low level which is held from that time on, corresponding to the fast scattering out of the tracer from the circle.

3.2 Mixing Depth of Fluorescent Sand Tracer in the Sea Bottom

As pointed out by *Komar* and *Inman* (1970) and *Kraus* (1985), a phenomenon of sand

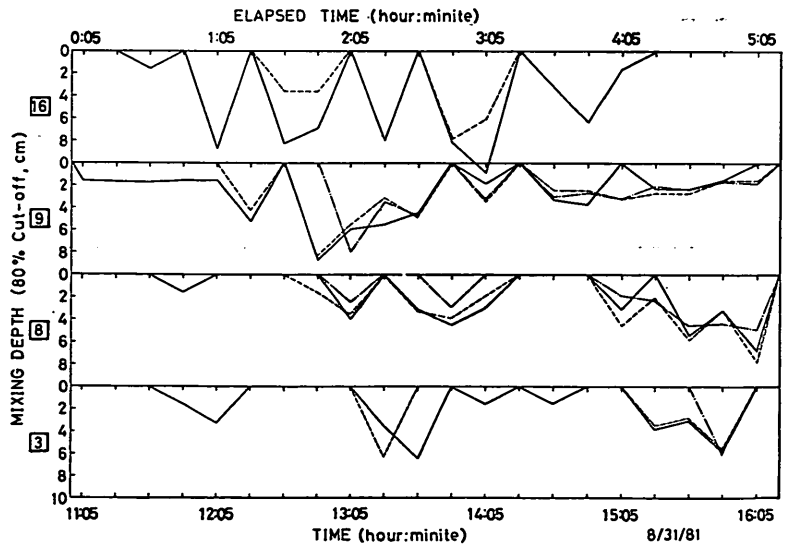

Fig.27 Change of the mixing depth of tracer with respect of time at the representative four points (8/31/81, Oarai Beach).

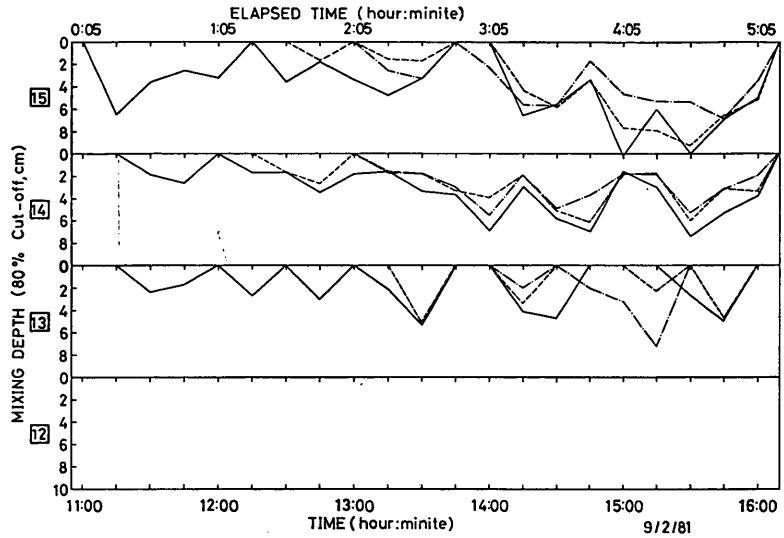

Fig.28 Change of the mixing depth of tracer with respect of time at the representative four points (9/2/81, Oarai Beach).

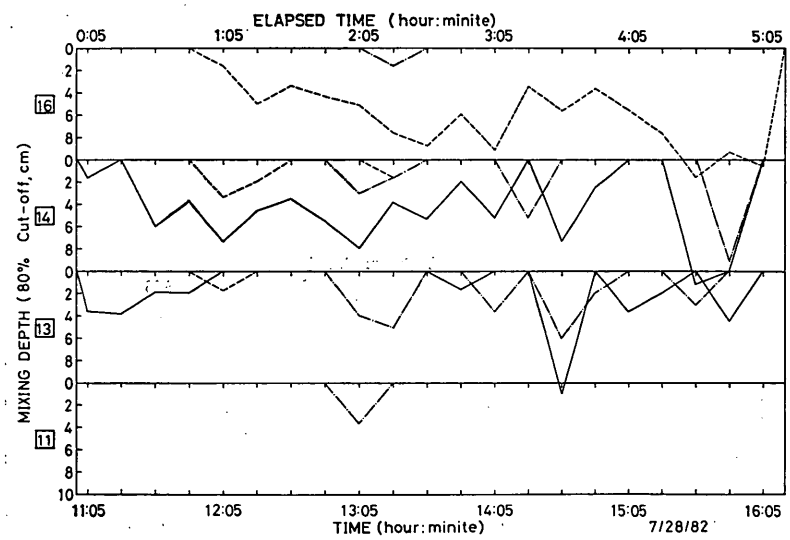

Fig.29 Change of the mixing depth of tracer with respect of time at the representative four points (7/28/82, Sudahama Beach).

mixing in a layer from the sea bottom surface to some depth exists in the surf zone. Among the sixteen sampling points, four points are chosen which indicated the largest four values of the total count number of tracer. The mixing depth of the fluorescent sand tracer at the representative four points are shown with respect to time in Fig. 27 through Fig.33. In these figures, the upper-side abscissa indicates the elapsed time and the lower-side one is the actual time. The figure bounded with a square on the left-

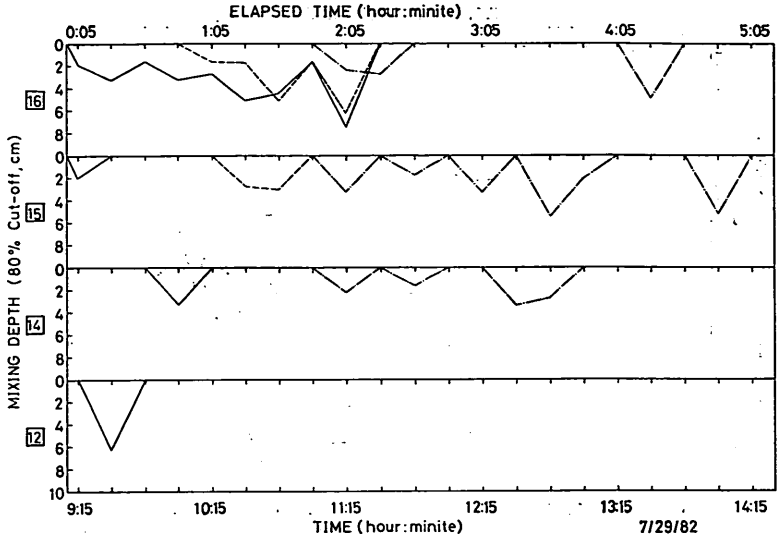

Fig.30 Change of the mixing depth of tracer with respect of time at the representative four points (7/29/82, Sudahama Beach).

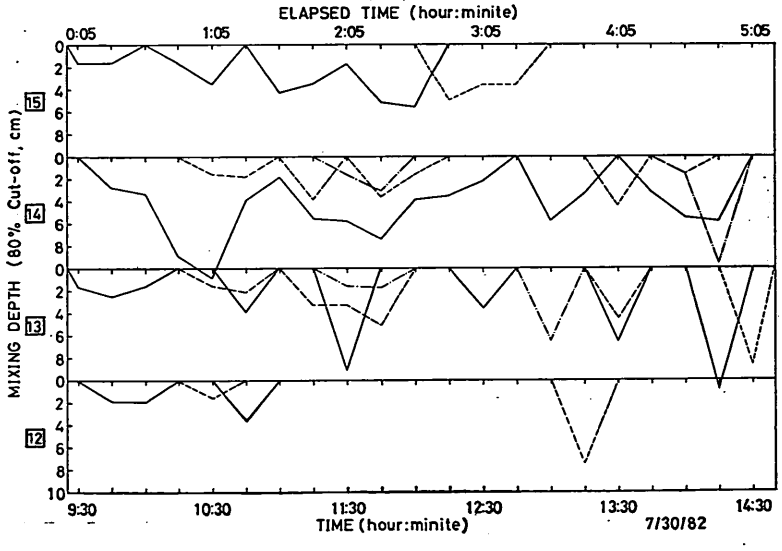

Fig.31 Change of the mixing depth of tracer with respect of time at the representative four points (7/30/82, Sudahama Beach).

hand side is the reference number of sampling point. Solid lines, broken lines and dashdot lines correspond to the mixing depth changes of the first, the second and the third injected tracer, respectively. In this report the mixing depth is defined as the depth containing 80% of the total tracer in a core, in the same manner as *Kraus* (1985).

According to these figures, we can make statements on the feature of mixing process of fluorescent sand tracer as follows :

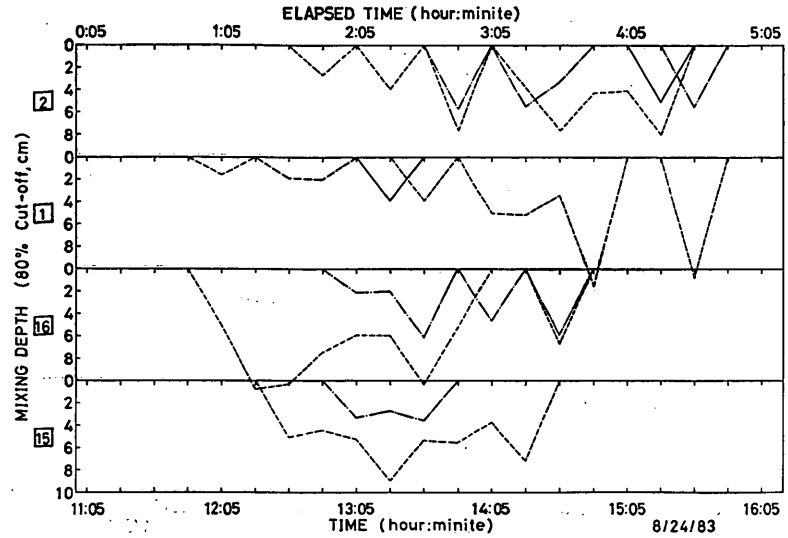

Fig.32 Change of the mixing depth of tracer with respect of time at the representative four points (8/24/83, Sudahama Beach).

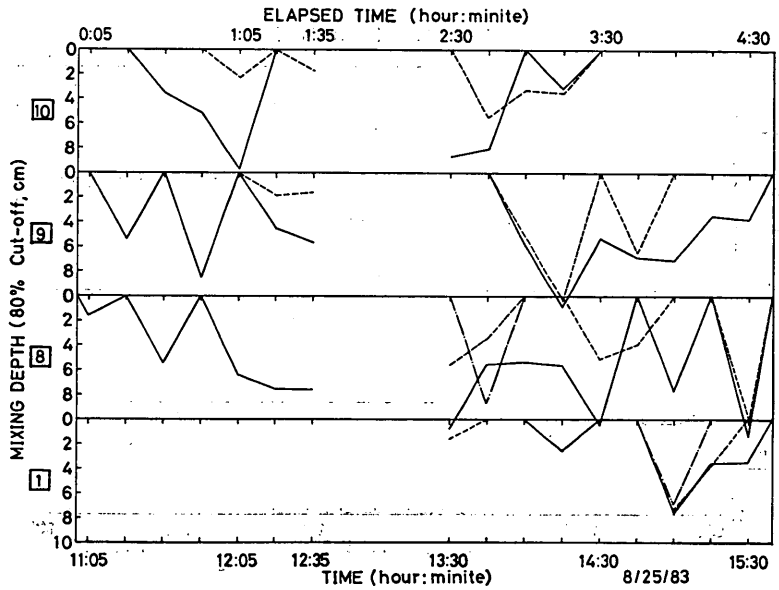

Fig.33 Change of the mixing depth of tracer with respect of time at the representative four points (8/25/83, Sudahama Beach).

(a) The mixing depths of three kinds of tracer change in the same way with time, being not influenced much by the intermittent injections of tracer in the cases of 8/31/81 and 9/2/81.

(b) The tracer injected earlier has a tendency to be more deeply buried during the observations in 1982 and 1983, when the mean current velocities were strong. Typical examples are those at the sampling points of No.14 in 7/28/82, No.14 in 7/30/82, No.15

and 16 in 8/24/83 and No.8, 9 and 10 in 8/25/83.

(c) In the case of 8/24/83, the first injected tracer is scarcely buried into the sea bottom, although both the second and the third injected tracer are buried. As seen in Fig.25, the first injected tracer are found only a little on the circumference. Therefore,

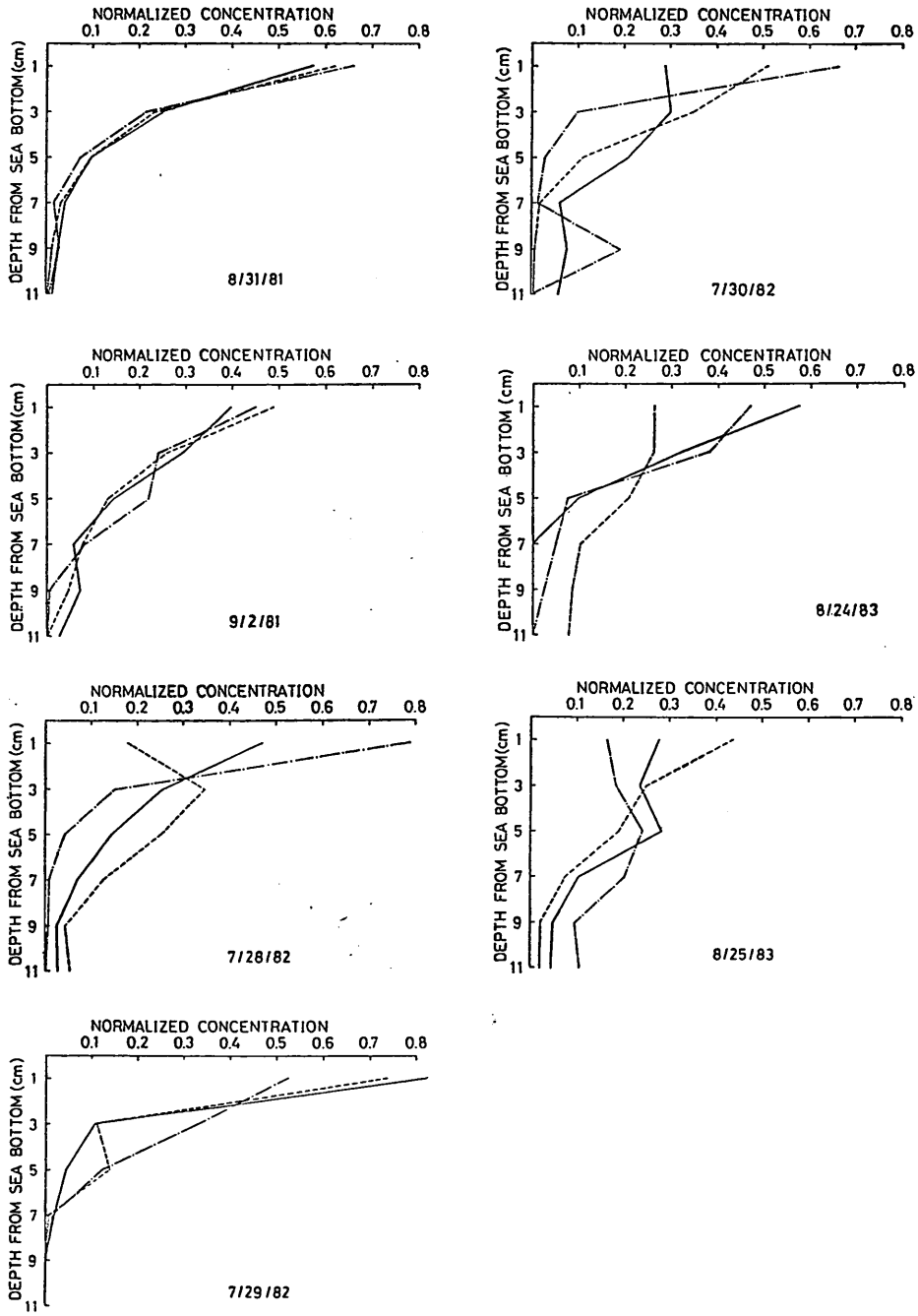

Fig.34 Vertical distribution of the fluorescent sand tracer in the sea bottom, averaged for all data.

the tracer must have been transported very fast to the outside of circumference in a state of thin layer on the sea bottom or suspension in the water during a period of just after its injection when it was shallow with the depth of probably 10 to 20 cm at low tide.

The vertical distributions of fluorescent sand tracer are calculated for each tracer with all of the data, and the result is illustrated in Fig.34 after the tracer concentrations having been normalized with the respective total values. The average mixing depth of 80% cut-off are also calculated and listed in Table 3.

Table 3 Mixing depth of 80% cut-off on the average (cm).

	1st	2nd	3rd
8/31/81	4.08	3.37	3.64
9/ 2/81	4.09	3.96	3.60
7/28/82	4.89	4.89	3.77
7/29/82	3.59	3.16	3.13
7/30/82	4.32	3.60	3.67
8/24/83	3.22	5.48	4.02
8/25/83	5.62	4.79	6.53

The mixing depth of tracer is governed by the process of sand mixing beneath the bottom. This is true at least for the cases in which the sea bottom was slightly eroded during the observation as evidenced by the measurements of clearance between the sea bottom and the sensor of the currentmeter, because the sand did not deposit on the bottom in these cases (see Table 2). The relation between the mixing depth and the external forces of current velocities will be discussed in Chapter 4.

3.3 Characteristics of Waves and Currents

The current velocities were measured by an electromagnetic currentmeter of two-component type at the injection point of tracer. The orientation of the horizontal axis of the currentmeter was measured by means of a transit surveying from the two points on the land in the same manner as explained in the first report. The orientation of currentmenter can be measured more precisely by this method than by a magnetic compass in the sea water. The data of these velocities were recorded on an analogue magnetic tape in the field and digitized at the interval of 0.1 second in a laboratory. Every two consecutive digital data are averaged to yield the smoothed data with the time interval of 0.2 second, which are utilized for analyses.

The representative values of currents, that is to say, the mean velocity, the principal direction of the incident waves, the skewness, the long-crestedness and the root-mean-square value of velocity fluctuation in the principal wave direction, are calculated for every fifteen minutes by using the following equations.

The mean velocity is defined as

$$\overline{V}=\sqrt{\overline{u^2}+\overline{v^2}}, \qquad (3)$$

where u and v are the horizontal components of the current velocities and an overbar in expression means the time average.

The long-crestedness is a parameter which indicates a degree of concentration of wave directions : $\gamma^*=0$ for the waves with infinitely long crests, and $\gamma^*=1$ for the waves of completely random directionality (*Nagata* 1964). The long-crestedness can be evaluated by

$$(\gamma^*)^2=\frac{(\overline{u^2}+\overline{v^2})-\sqrt{(\overline{u^2}-\overline{v^2})^2+4\overline{uv}^2}}{(\overline{u^2}+\overline{v^2})+\sqrt{(\overline{u^2}-\overline{v^2})^2+4\overline{uv}^2}}, \tag{4}$$

where u and v are not original values but the components of wave motions only, which are obtained by removing the steady state currents from the original data.

A principal direction of the waves, θ_p, is defined as

$$\tan 2\theta_p=\frac{2\overline{uv}}{\overline{u^2}-\overline{v^2}}. \tag{5}$$

Equation (5) cannot make a distinction between the waves travelling in opposite directions. In this study, however, we can uniquely determine the wave direction because the observation sites were located in the surf zone and the waves came only from the offshore to the nearshore.

The velocity component in the principal wave direction U_p, being defined positive in the direction of wave propagation, can be obtained by the coordinate transformation with the angle of θ_p. The skewness is defined for U_p as

$$\sqrt{\beta_1}=\frac{1}{(U_p)^3_{\mathrm{rms}}}\cdot\frac{1}{N}\sum_{i=1}^{N}[(U_p)_i-\overline{U_p}]^3, \tag{6}$$

where the root-mean-spuare value of U_p is given by

$$(U_p)_{\mathrm{rms}}=\sqrt{\frac{1}{N}\sum_{i=1}^{N}[(U_p)_i-\overline{U_p}]^2}\equiv\sqrt{\overline{U_p{}^2}}. \tag{7}$$

The results of analyses on waves and currents are shown for each case in Fig.35 through Fig.41. The calculated values are plotted at the end of every fifteen minutes. For example, the values at the actual time of 10 : 50 in the case of 8/31/81 (Fig.35) are those calculated for a period during 10 : 35 to 10 : 50. The first values in each case, however, are those calculated for five minutes just after the first injection. An exception is for the values at the actual time of 12 : 45 in 8/25/83 (Fig.41), which are calculated for ten minutes from 10 : 35 to 10 : 45. The directions of the mean currents and the principal directions of the incident waves are defined with angles in the clockwise direction from the sampling point of No.1 as shown in Fig.1. The origin of the ordinate for the skewness is different for each case. Therefore, the location of the origin should be confirmed before inspecting the skewness in every case.

On Fig.35 through Fig.41, we can make the following statements, which are restricted to important features of each case :

[8/31/81, Oarai Beach, Fig.35]

The mean velocity is mostly less than 10 cm/s, which is the weakest in all of the observations. Furthermore, the direction of mean current velocity changes in the counterclockwise direction from 360 degrees (offshore) to 0 degree at the actual time of 10 : 30 and offshore again at that of 13 : 50. This feature of mean current velocity is in

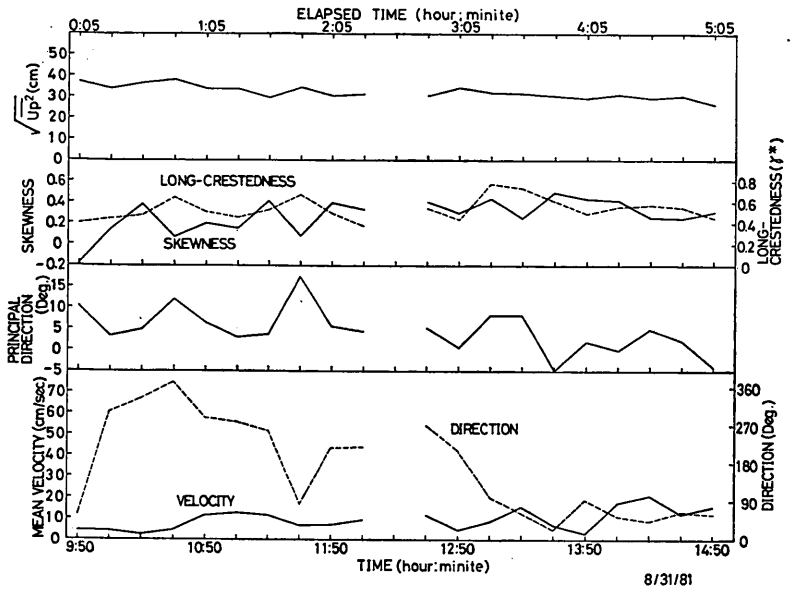

Fig.35 Characteristics of waves and currents during the observation in 8/31/81, Oarai Beach.

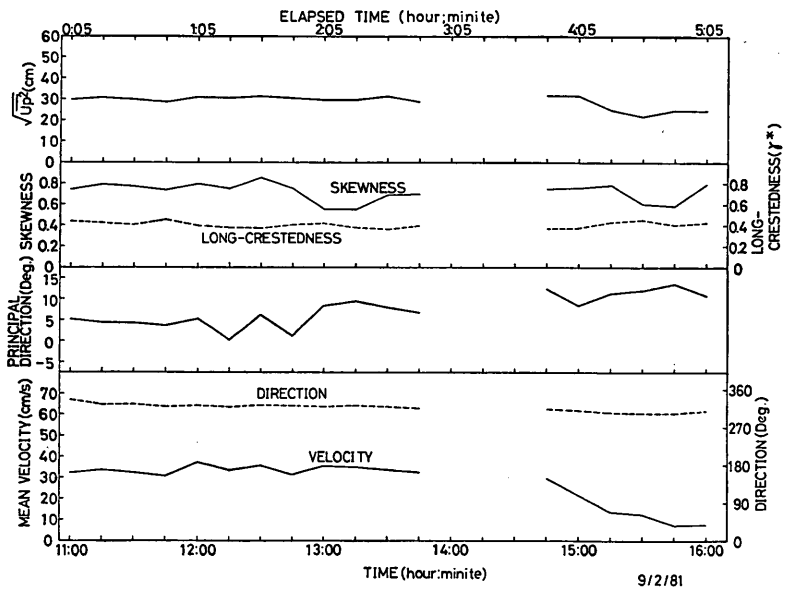

Fig.36 Characteristics of waves and currents during the observation in 9/2/81, Oarai Beach.

agreement with the dispersion of the fluorescent sand tracer in all directions (see Fig. 12).

[9/2/81, Oarai Beach, Fig.36]

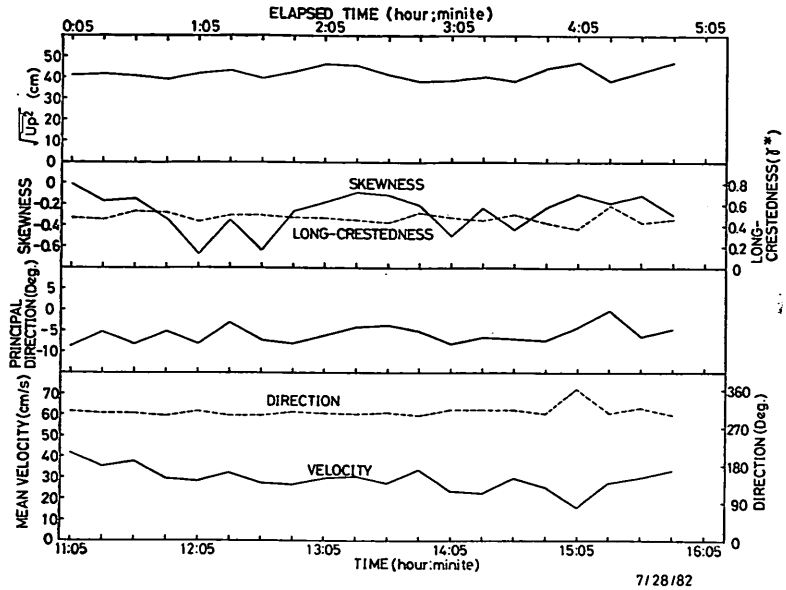

Fig.37 Characteristics of waves and currents during the observation in 7/28/82, Sudahama Beach.

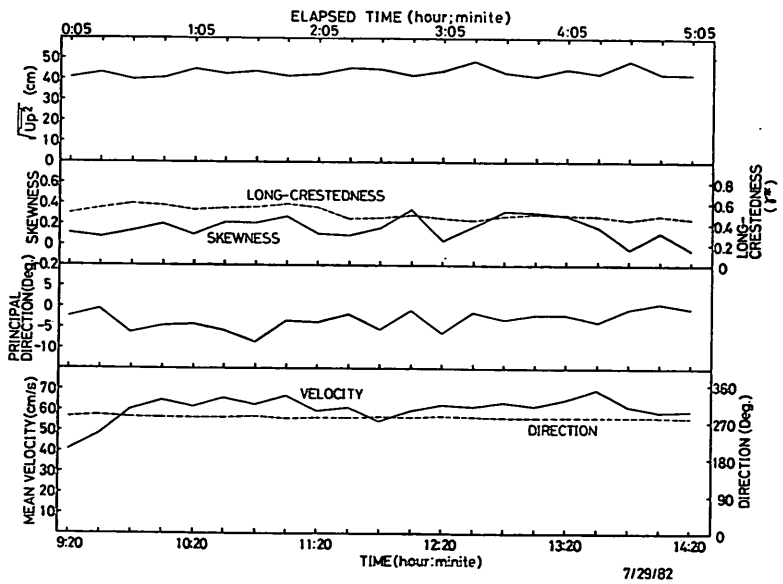

Fig.38 Characteristics of waves and currents during the observation in 7/29/82, Sudahama Beach.

In this case the value of skewness is large, 0.73 on the average, compared with other observations, while the value of long-crestedness is the smallest which means that uni-directionality of waves is the most predominant. Although the direction of mean current

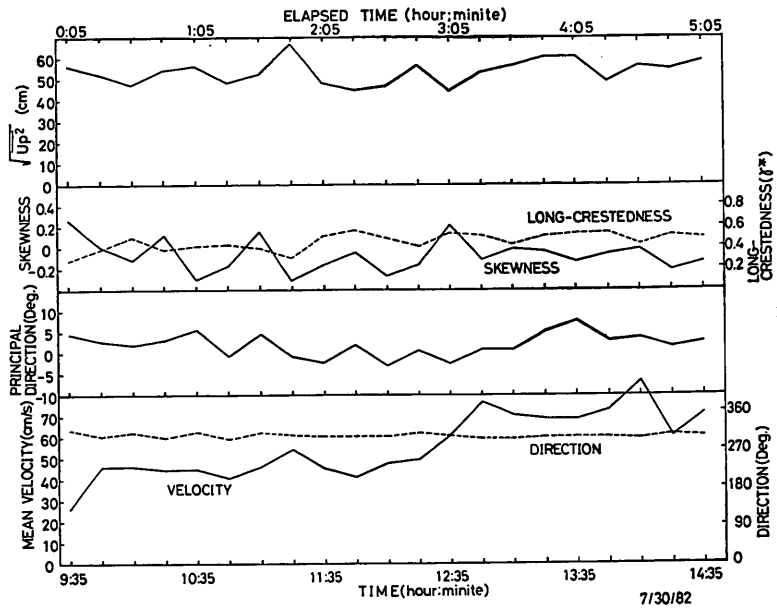

Fig.39 Characteristics of waves and currents during the observation in 7/30/82, Sudahama Beach.

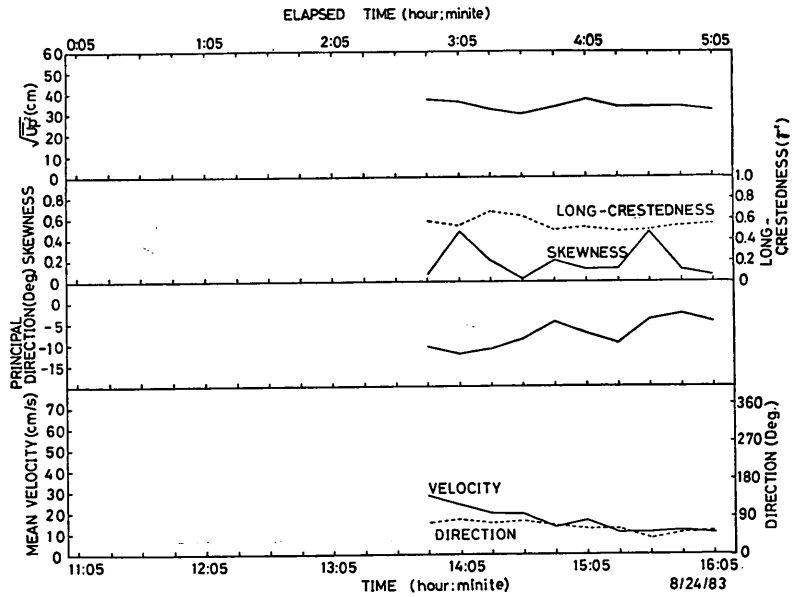

Fig.40 Characteristics of waves and currents during the observation in 8/24/83, Sudahama Beach.

is held constant and its velocity is more than 30 cm/s in the first half, the velocity begins to gradually decrease after the actual time of about 14 : 45 to the value less than 10 cm/s at the end of observation.

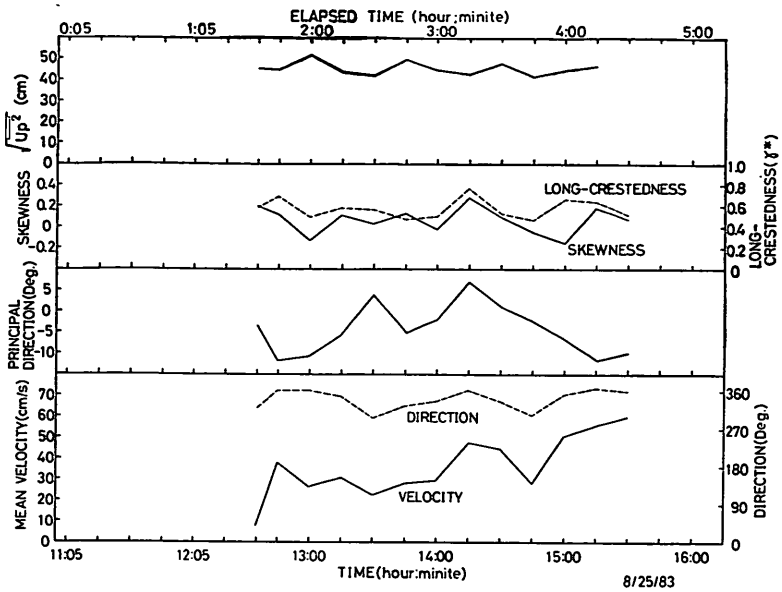

Fig.41 Characteristics of waves and currents during the observation in 8/25/83, Sudahama Beach.

[7/28/82, Sudahama Beach, Fig.37]

The most important feature in this case is that the value of skewness is usually negative, a cause of which must be examined in detail later.

[7/29/82, Sudahama Beach, Fig.38]

The mean current velocity is the strongest, 60.2cm/s on the average, among all the observations, and it shows little change of the direction. The value of skewness is rather small, being 0.15 on the average.

[7/30/82, Sudahama Beach, Fig.39]

The mean velocity of about 40cm/s at the start of the observation gradually increases to about 70 to 80cm/s by the end of observation. During this period, the direction of the mean velocity is held constant. Furthermore, the root-mean-square value of velocity fluctuation in the principal direction of the incident waves is the largest among all the observations. The value of skewness frequently becomes negative, yielding the value of -0.07 on the average.

[8/24/83, Sudahama Beach, Fig.40]

The measurement of currents did not go well during the first half because of the noises in the record owing to the emergence of the sensor of currentmeter above the sea surface during the low tide level, and only the data in the latter half are available. As for the latter data, the mean velocity is small and it decreases with time.

[8/25/83, Sudahama Beach, Fig.41]

The measurement of currents did not go well during the first period of about one and half hours due to the same reason as that in 8/24/83. The mean velocity continuously increases from the value less than 10cm/s at the actual time of 12 : 35 to that of about 60cm/s at the end of observation. During this period, the direction of the mean current is almost 360 degrees (offshore) which indicates that there existed rip currents at the observation point. Because of this, a frogman was carried by them to the offshore, which disturbed the work of sampling during the actual time of 12 : 30 to 13 : 30.

After that, the work of taking core samples was restarted, but we could not help giving up to continue them at the actual time of 15 : 45 because the rip currents became too strong with time and it was considered to be very dangerous for the frogmen.

For every observation, the arithmetic means of the representative characteristics of waves and the vectorial means of the mean current velocities and their directions are calculated, and the resultant values are listed in Table 2.

According to Table 2, the mean values of skewness in 7/28/82 and 7/30/82 are negative, and those in 7/29/82, 8/24/83 and 8/25/83 are positive but small. On the other hand, those in 8/31/81 and 9/2/81 on Oarai Beach are positive and large. The result of the measurement at Ajigaura Beach also shows large positive values of the skewness except for the data of 3/2/80. As the velocity fluctuation due to waves U_p is defined as positive in the direction of wave propagations in these data analyses, the values of the skewness of U_p in the surf zone would be thought positive and large from the analogy of surface wave profiles ; that is to say, the onshore velocities are typically stronger and of shorter duration than those of the offshore flows. It is a quite curious fact that the mean values of skewness are small positive or negative on Sudahama Beach. Their cause is examined here.

Figures 42 and 43 show typical records of current variations. They are five minutes segments of the records of Oarai Beach on 9/2/81 and Sudahama Beach on 7/30/82, respectively. The direction of the Y-component is almost the same as the direction of the incident wave propagation and that of the X-component is normal to the Y-component or nearly parallel to the shoreline. In the case of 9/2/81 (Fig.42), the velocity fluctuation is mainly due to the incident waves and the value of skewness is large, being 0.72 on the

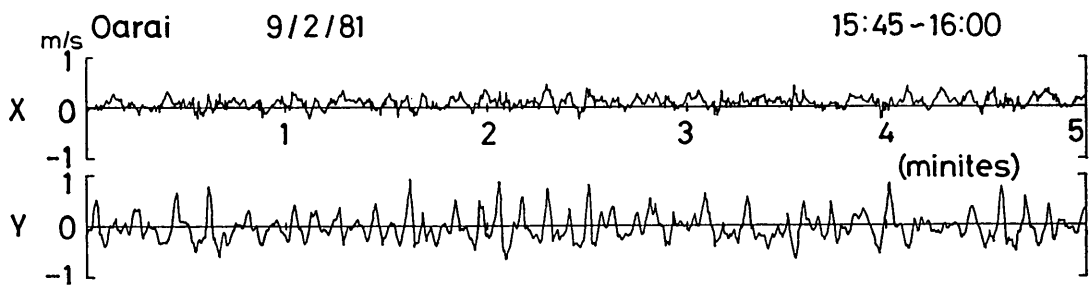

Fig.42 Typical segment of current records (9/2/81, Oarai Beach).

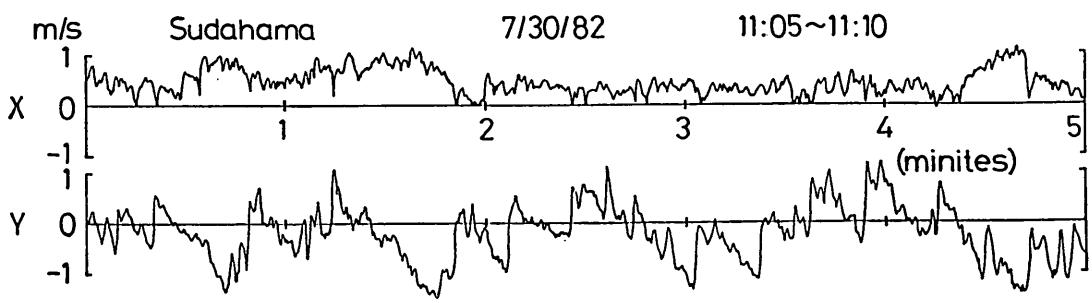

Fig.43 Typical segment of current records (7/30/82, Sudahama Beach).

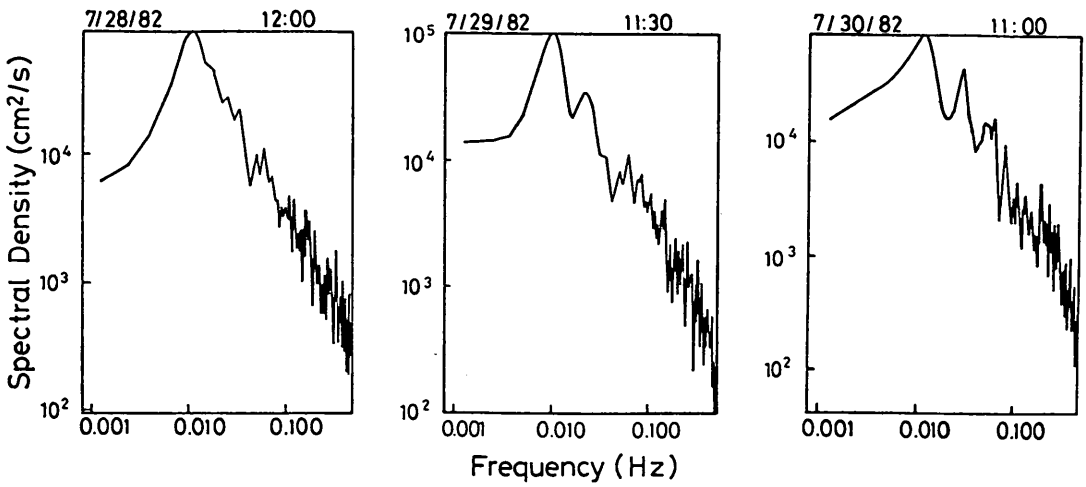

Fig.44 Spectral densities of velocity fluctuations in the principal direction of the incident waves in 1982, Sudahama Beach.

average. In the case of 7/30/82 (Fig.43), however, the current velocity in the Y-component is featured with the existence of long-period fluctuations which have the period of about 80 to 100 seconds and the amplitude much greater than that of the short-period fluctuations corresponding to the motions of incident waves. The value of skewness is negative in the latter case as previously explained.

Spectral analyses have been made for the velocity components in the principal direction. The data sampling interval is $\Delta t=0.4$ s and the number of data is $N=2048$ for the duration of about 13 minutes and 40 seconds for each analysis. Figure 44 shows spectral densities of the velocities on Sudahama Beach in 1982. The experiment number and the start time of spectral analysis are presented on the upper-side of each figure. According to Fig.44, there are spectral peaks at the frequency of about 0.01 Hz, but no peak is recognized in the frequency band of 0.1 to 0.15 Hz which is corresponding to the periods of the incident waves. This is owing to the fact that the energy of the long-period fluctuations is so large to conceal the energy of the short-period fluctuations. The spectral analyses have also been done for the records obtained in 1981 and in 1983. The spectral peaks at the frequency of about 0.01 Hz are recognized in the records of 1983 on Sudahama Beach, but not in those of 1981 on Oarai Beach.

It can be inferred from the above results that the value of skewness is influenced not only by the contribution of the short-period components but also by that of the long-period components. For example, in the case that the amplitude of long-period fluctuation is greater than that of short-period one, the statistical distribution of instantaneous current velocity will be governed by that of the former fluctuations. By inspecting Fig.43 in detail, we can notice that the long-period components do not fluctuate sinusoidally but in the way that the velocity profile is flattened with longer duration in the positive side (onshore) and is sharpened with shorter duration in the negative side (offshore). Therefore, the value of skewness for the long-period components is considered to be negative, even if there exists the short-period components having the positive value of skewness.

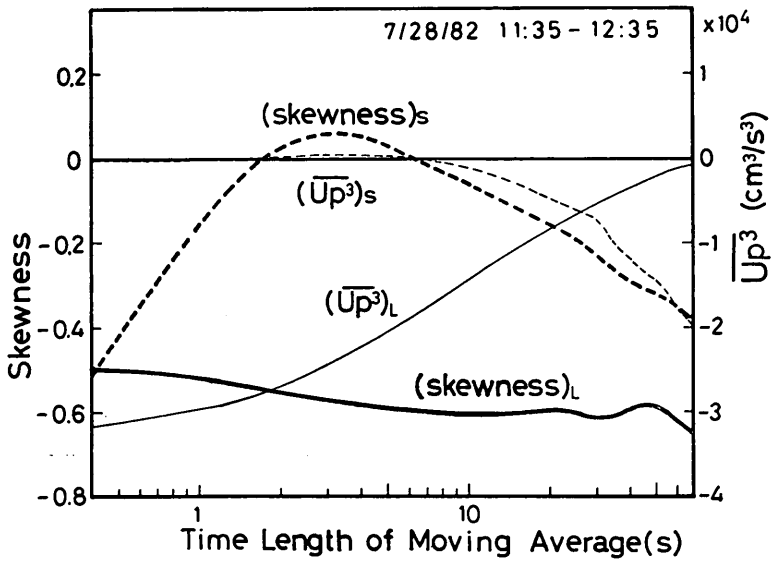

Fig.45 The values of skewness for the long period component and the short one (7/28/82, Sudahama Beach).

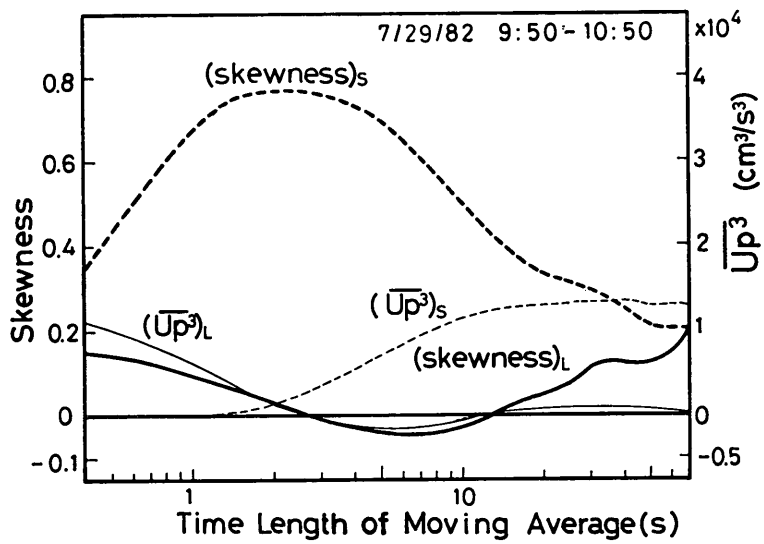

Fig.46 The values of skewness for the long period component and the short one (7/29/82, Sudahama Beach).

In order to confirm the above inference, two analyses have been attempted for calculating the values of skewness. One analysis is to calculate the value of skewness, which is denoted by $(\text{skewness})_L$, for the smoothed velocity profile which is obtained by the application of the moving average technique ; the averaging time length is varied from 0.45 s to 70 s. Another is to calculate the skewness for the profile with removal of the smoothed profile, which corresponds to that of the relatively short-period components, and the resultant value is denoted by $(\text{skewness})_S$. These analyses have been

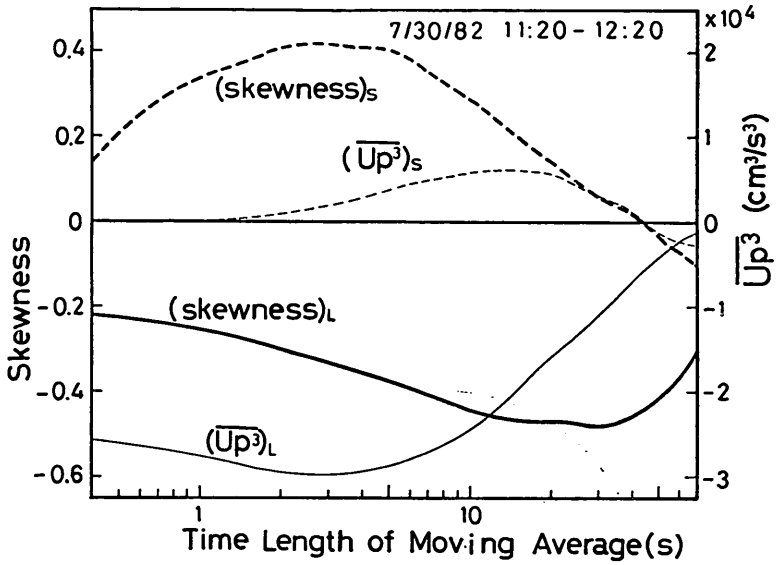

Fig.47 The values of skewness for the long period component and the short one (7/30/82, Sudahama Beach).

done for the time series data of one hour. The results of analyses for the cases of 7/28 /82, 7/29/82 and 7/30/82 are shown in Figs. 45, 46 and 47, respectively, where the abscissa denotes the averaging time length. According to these figures, the values of skewness for the short-period components are usually greater than those for the long-period components. Especially in the cases of 7/28/82 and 7/30/82, those for the long-period components are always negative.

There have been presented many papers showing the evidences of the presence of the long-period waves of one to several minutes in period coexisting with the incident waves in the surf zone : e.g., *Huntley* and *Bowen* 1973, *Suhayda* 1974, *Huntley* 1976, *Sasaki* and *Horikawa* 1978, *Holman*, *Huntley* and *Bowen* 1978, *Huntley* and *Bowen* 1978, *Hotta*, *Mizuguchi* and *Isobe* 1981, *Huntley*, *Guza* and *Thornton* 1981, *Katoh* 1981, *Guza* and *Thornton* 1982. To the knowledge of the authors, however, there is no report which demonstrates that the value of skewness of the velocity fluctuations of the long-period waves is negative.

As easily understood from Fig.43, it is meaningless to define individual waves for current fluctuations by applying the zero-upcrossing or zero-downcrossing method and to calculate the highest one-third amplitude of velocities when the data contain predominant long-period components, because there is no definite standard for removing the long-period components from the records. Therefore, in this report the root-mean-square value is employed as the measure of the magnitude of velocity fluctuations, instead of the highest one-third amplitude of velocitis, and it is indicated at the upper sections of Fig.35 through Fig.41.

The question whether the observed long-period velocity fluctuations are due to the edge waves or the reflected waves has not been studied, because we have only the current data measured at one point in the surf zone and are unable to scrutinize it.

4. Relation between Movements of Fluorescent Sand Tracer and Fluid Dynamics

4.1 Advection Speed and Its Direction of Fluorescent Sand Tracer

First of all, let us estimate the advection speed and its direction of sand tracer, utilizing the data shown in Sections 3.1 and 3.2. For this purpose, the following equations which have been derived in the first report [29] are employed here.

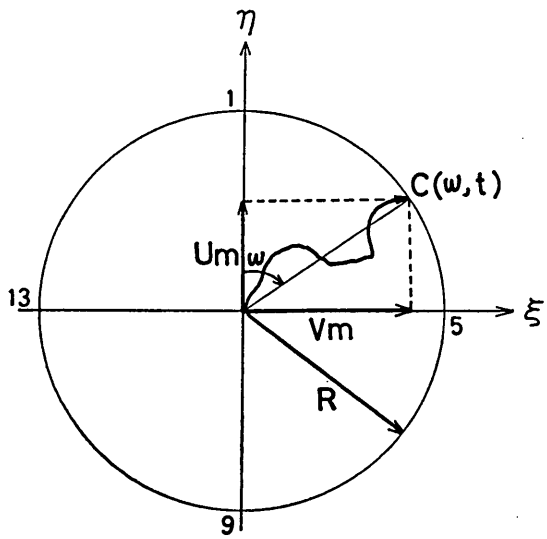

Fig.48 Coordinate system for calculation of the advection speed and its direction of tracer movement.

Let $C(\omega, t)$ be the number of tracer particles in a core at the time t after the injection of tracer at a point of the direction ω on the circumference having a radius R (see Fig.48). Up to this time, tracer particles of $C(\omega, t)$ in number are considered to have moved from the center of circle to the circumference. It does not matter how tracer particles were transported there, whether in suspension or not, what happened with them on the way, and which way did they pass through. We are only concerned with the fact that they have moved there with the travelling time of t. Then the components of apparent travelling speed of tracer particles in the directions of η and ξ are given by $(R\cos\omega)/t$ and $(R\sin\omega)/t$, respectively. Furthermore, the mean advection velocity of tracer during the experiment can be defined by the following two components, u_m and v_m :

$$u_m=\frac{\int_0^\infty\int_0^{2\pi}C(\omega,t)\frac{R}{t}\cos\omega d\omega dt}{\int_0^\infty\int_0^{2\pi}C(\omega,t)d\omega dt}\ , \tag{8}$$

$$v_m=\frac{\int_0^\infty\int_0^{2\pi}C(\omega,t)\frac{R}{t}\sin\omega d\omega dt}{\int_0^\infty\int_0^{2\pi}C(\omega,t)d\omega dt}\ . \tag{9}$$

By using Eqs. (8) and (9), we have

$$V_t = \sqrt{u_m^2 + v_m^2}, \tag{10}$$

$$\theta_t = \tan^{-1}(v_m/u_m), \tag{11}$$

where V_t is the mean advection speed of fluorescent sand tracer and θ_t is its direction, being defined in the same manner as ω.

Because the data available are discrete values both in time and in space, Eqs. (8) and (9) must be rewritten as follows :

$$u_m = \frac{\sum_{ti=1}^{n_t}\sum_{\omega j=1}^{n_\omega} C(\omega_j, t_i)\frac{R}{T_i}\cos\omega_j \Delta\omega\Delta t}{\sum_{ti=1}^{n_t}\sum_{\omega j=1}^{n_\omega} C(\omega_j, t_i)\Delta\omega\Delta t}, \tag{12}$$

$$v_m = \frac{\sum_{ti=1}^{n_t}\sum_{\omega j=1}^{n_\omega} C(\omega_j, t)\frac{R}{T_i}\sin\omega_j \Delta\omega\Delta t}{\sum_{ti=1}^{n_t}\sum_{\omega j=1}^{n_\omega} C(\omega_j, t_i)\Delta\omega\Delta t}, \tag{13}$$

where

Δt : sampling interval equal to 5 minutes for the first sampling and 15 minutes

Table 4 Advection speed and its direction of sand tracer (Symbols are defined in Fig.48).

		u_m(cm/m)	v_m(cm/m)	V_t(cm/m)	θ_t(Deg)
8/31/81	1	− 8.08	− 6.04	10.09	216.8
	2	−13.99	− 4.05	14.56	196.1
	3	−11.90	0.30	11.90	178.6
9/ 2/81	1	3.87	− 6.33	7.42	301.4
	2	3.58	− 6.98	7.84	297.1
	3	5.65	− 9.40	10.97	301.0
7/28/82	1	9.63	−24.11	25.96	291.8
	2	11.80	− 9.26	15.00	321.9
	3	18.40	−51.47	54.66	289.7
7/29/82	1	86.05	−15.74	87.48	349.6
	2	51.97	−23.57	57.07	335.6
	3	24.29	−22.06	32.81	317.8
7/30/82	1	4.74	−13.55	14.36	289.3
	2	7.42	−25.22	26.29	286.4
	3	6.67	−36.43	37.04	280.4
8/24/83	1	1.29	−17.05	17.10	274.3
	2	19.21	−16.11	25.07	320.0
	3	13.72	− 6.07	15.00	336.1
8/25/83	1	− 6.01	− 2.08	6.36	199.1
	2	− 8.70	− 7.75	11.65	221.7
	3	7.31	1.34	7.43	10.4

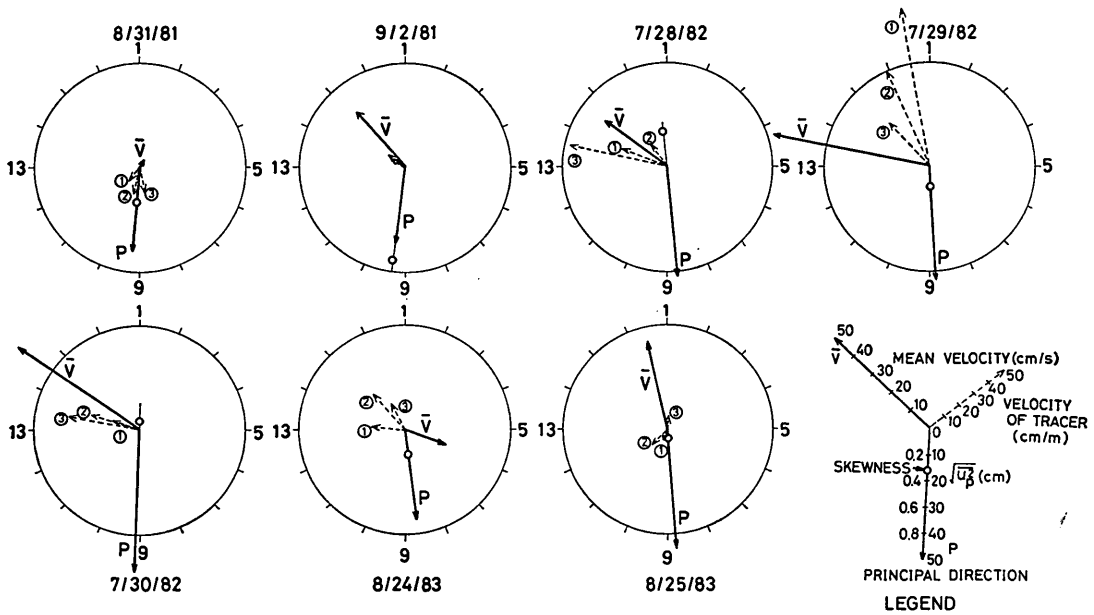

Fig.49 Advection speed and its direction of tracer movements, representative features of currents and waves.

for remaining ones,

$\Delta\omega$: angle between successive two sampling points, being 22.5 degrees,

n_ω : number of sampling points, being 16,

n_t : number of sampling times, being 21, 17 and 13 for the first, the second and the third injected tracers,

$C(\omega_j, t_i)$: number of tracer particles in a core sample on the ω_j-th point on the circumference at the t_i-th sampling time,

T_i : elapsed time from the tracer injection, being equal to $5+(t_i-1)\cdot 15$ minutes.

The mean advection speed of tracer and its direction are calculated by applying these equations to the tracer data and the resultant values are listed in Table 4 and shown by vectorial expressions with broken arrows in Fig.49. The figures surrounded by small circles in Fig.49 correspond to the order number of tracer injection. The representative characteristics of currents and waves, which are the averaged values during each observation (see Table 2), are also shown in Fig.49. The mean current velocity is represented by the solid arrow with the symbol "$\overline{V}$", the length of which corresponds to the magnitude of its velocity. The principal direction of the incident waves is represented by the solid arrow with the symbol "P", the length of which corresponds to the root-mean-square value of velocity fluctuations in that direction. A small open circle on the arrow of the principal wave direction indicates the magnitude of the value of skewness by its position relative to the origin. The open circle plotted on the side of the principal wave direction has a positive value of skewness, whereas that plotted on the opposite side has a negative value. Scales of these arrows are indicated in the legend on the lower-right corner.

Although the tracer advection must be governed by the external forces of the mean current and the velocity fluctuation due to incident waves, it is rather difficult to

observe clear relations between the tracer advection direction and the mean current direction or the principal wave direction in Fig. 49. Then, the relation between the tracer advection and the characteristics of waves and currents will be discussed hereinafter.

4.2 Coordinate System for Analyses

The motion of an object is often analyzed by decomposing it into two perpendicular linear components. The technique may not be applicable for the case of fluid motion in the analysis of sand transport rate, because it is considered that the time averaged sediment transport rate depends on the higher moments of fluid velocity (e.g., *Bowen* 1980, *Bailard* 1981). However, the authors will employ the decomposition technique as the first approximation to the analysis of sand transport rate.

In the study of sand transports, one of the two kinds of coordinate systems is usually employed. One coordinate system is such that an axis is taken parallel to the shoreline (in the longshore direction) and another one to be perpendicular to the shoreline (in the offshore direction). The other coordinate system is such that an axis is taken in the principal direction of the incident waves, and another one is taken normally to it. In this study, however, an oblique coordinate system which has been introduced in the first report [29] will be used again. That is to say, the η axis is taken in the principal wave direction and the ξ axis is taken in the mean current direction, as shown in Fig.50. As these two axes generally intersect at an oblique angle, let the angle

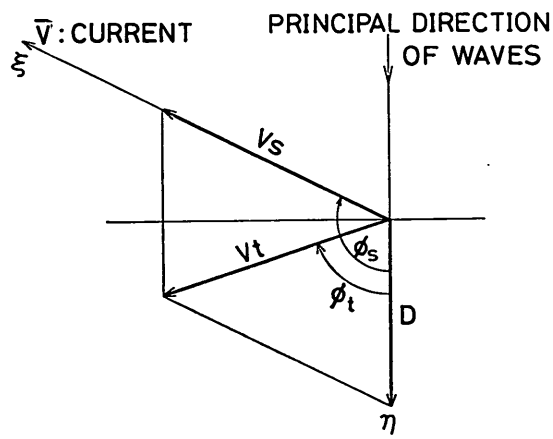

Fig.50 Oblique coordinate system and definition of symbols.

measured from the η axis to the ξ axis in the clockwise direction be ϕ_s. The oblique system is considered to be more useful in this case, because the directions of two axes are in agreement with those of external forces and thus it becomes easy to examine the relationships between the tracer advection and the characteristics of currents and waves.

Let us assume that the sand advection speed is V_t with the angle ϕ_t, which is defined in the same way as ϕ_s. Furthermore its two components in the directions of the mean current and the wave propagation are denoted by V_s and D, respectively, as shown in Fig.50. Then we have two equations as follows :

$$D+V_s\cdot\cos\phi_s=V_t\cdot\cos\phi_t, \tag{14}$$

in the principal direction of the incident waves and

$$V_s\cdot\sin\phi_s=V_t\cdot\sin\phi_t, \tag{15}$$

in the direction normal to the principal wave direction. As Eqs. (14) and (15) are simultaneous equations for V_s and D, we have

$$V_s=V_t\cdot\frac{\sin\phi_t}{\sin\phi_s}, \tag{16}$$

$$D=V_t\cdot\cos\phi_t\cdot\left(1-\frac{\tan\phi_t}{\tan\phi_s}\right). \tag{17}$$

Table 5 Tracer advection speed and representative value of currents and waves.

Experiment Number		$\overline{V}$ (cm/s)	V_s (cm/s)	D (cm/s)	$\sqrt{\overline{U_p{}^2}}$ (cm/s)	Velocity Skewness	$\sqrt{\overline{\dot{U}_p{}^2}}$ (cm/s)	Velocity Atiltness
2/29/80		8.00	0.301	0.120	27.68	0.344	46.16	0.472
3/ 1/80		10.40	0.167	0.262	29.02	0.452	48.57	0.521
3/ 2/80		14.00	0.282	−0.061	41.33	−0.013	47.80	1.281
9/ 1/80	1	49.00	0.691	0.169	42.20	0.425		
	2	49.00	0.598	0.178	42.20	0.425		
	3	49.00	0.379	0.118	42.20	0.425		
8/31/81	1	2.27	−0.224	−0.063	32.20	0.273	48.95	0.206
	2	2.90	−0.100	0.151	31.20	0.316	47.45	0.177
	3	5.37	0.019	0.209	30.66	0.354	44.85	0.101
9/ 2/81	1	27.48	0.151	0.050	28.93	0.719	60.45	0.954
	2	26.23	0.158	0.056	28.70	0.709	61.20	0.874
	3	22.94	0.208	0.053	27.92	0.677	63.30	0.725
7/28/82	1	22.88	0.516	0.145	41.96	−0.266	58.00	0.408
	2	27.15	0.183	−0.086	42.31	−0.289	58.20	0.406
	3	30.14	1.054	0.271	45.97	−0.131	56.90	0.434
7/29/82	1	49.53	0.188	−1.393	40.97	0.101	44.55	1.040
	2	62.82	0.319	−0.806	43.00	0.195	44.40	1.068
	3	61.17	0.360	−0.334	43.91	0.138	43.80	1.069
7/30/82	1	55.39	0.269	0.070	53.40	−0.069	43.50	1.075
	2	58.94	0.498	0.150	53.60	−0.102	44.60	1.002
	3	63.01	0.717	0.281	52.88	−0.086	45.95	0.951
8/24/83	1							
	2							
	3	15.97	−0.073	−0.255	33.99	0.190	55.30	0.506
8/25/83	1							
	2							
	3	36.11	−0.182	−0.299	45.00	0.049	46.20	0.930

As all of physical quantities in the right-hand sides in Eqs. (16) and (17) can be estimated by Eqs. (5), (10) and (11) by utilizing the data measured, the values of V_s and D have been calculated and are listed in the second and the third columns in Table 5. The calculation for each tracer was done by utilizing the representative values of waves and currents averaged for the period from the time of injection to the end of each observation (see Fig.51).

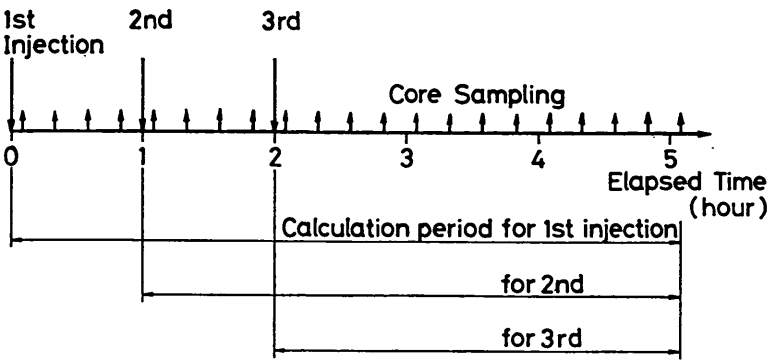

Fig.51 Calculation period for waves and currents.

4.3 Advection Speed of Sand Movement in the Direction of Mean Currents

In this section, the abvection speed of tracer in the direction of mean currents V_s is examined in terms of the mean current velocity $\overline{V}$.

The values of V_s and $\overline{V}$, which are listed in Table 5, are plotted in Fig.52. As seen in Fig.52, the data points, except one point which have relatively larger values of V_s, scatter around a straight line of

$$V_s=0.01\cdot\overline{V}. \tag{18}$$

Equation (18) is based on the derivation which makes use of the longshore sand transport formula in the first report [29]. Because the first report was written in Japanese, the derivation is followed here again by taking the latest knowledge into account.

According to *Komar* and *Inman* (1970), the bulk volume sand transport rate S_l and the immersed weight transport rate I_l along the beach are given by

$$S_l=\overline{b}\cdot X_b\cdot\overline{V_s}, \tag{19}$$

$$I_l=(\rho_s-\rho)ga'S_l, \tag{20}$$

where $\overline{b}$ is the average thickness of mixing layer on the beach face in the surf zone, X_b is the width of the surf zone, $\overline{V_s}$ is the mean advection speed of longshore transport, ρ_s and ρ are the sand and water densities respectively, a' is the correction factor for pore space and can be taken as 0.6, and g is the acceleration of gravity.

Kraus (1985) recently reported the relation between the average surf-zone mixing depth $\overline{b}$ and the significant breaking-wave height H_b as

$$\overline{b}=0.027\cdot H_b. \tag{21}$$

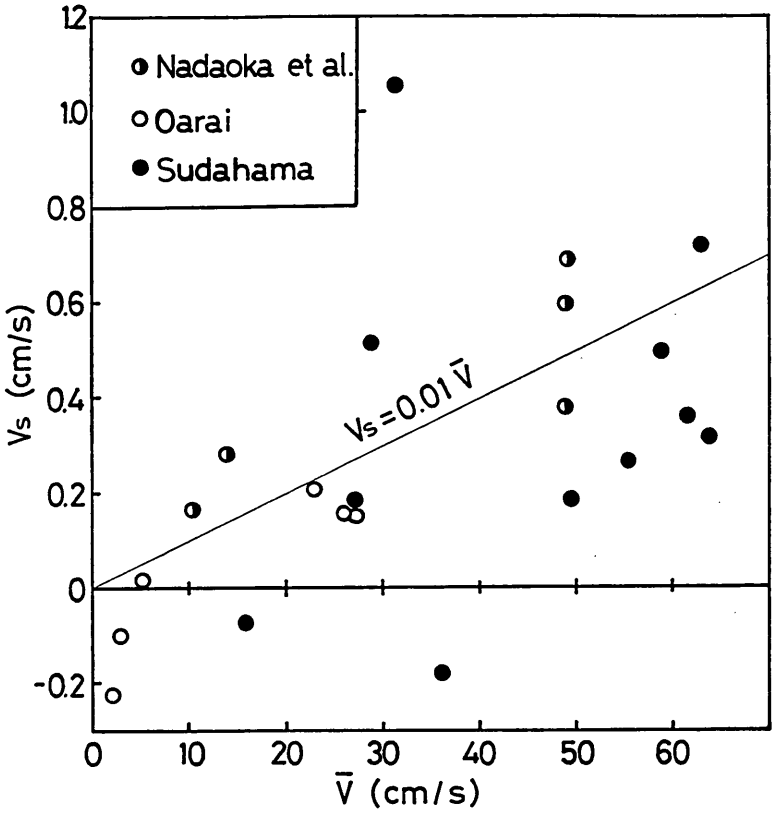

Fig.52 Sand tracer advection speed in the mean current direction compared with mean current velocities.

Now, let us assume that the mean advection speed of longshore sand transport is proportional to the longshore current velocity with the proportional coefficient of α as

$$\overline{V_s}=\alpha\overline{V_l}, \tag{22}$$

where $\overline{V_l}$ is the average longshore current velocity, which has been obtained by *Longuet-Higgins* (1970) (see *Komar* and *Inman* 1970) as

$$\overline{V_l}=\frac{5\pi}{8}\cdot\frac{\tan\beta}{C_f}\cdot u_b\cdot \mathrm{sim}\alpha_b\cos\alpha_b, \tag{23}$$

where $\tan\beta$ is the beach slope, assumed to be constant, C_f is the bottom frictional drag coefficient, u_b is the maximum horizontal component of the orbital velocity of the waves at the breaking point and α_b is the breaker angle. The maximum horizontal component of the orbitol velocity for the significant wave is given by the linearized wave theory as

$$u_b=\frac{1}{2}\gamma_b\cdot C_b, \tag{24}$$

where γ_b is a ratio of wave height to the water depth ($=H_b/h_b$) and C_b is the wave celerity at the breaking point. If we assume the constant bottom slope, an equation of

$$X_b \cdot \tan\beta \fallingdotseq h_b = H_b/\gamma_b \tag{25}$$

is valid approximately.

By substituting Eq. (21) through Eq. (25) into Eq. (20) and putting $a'=0.6$ and $\rho_s/\rho=2.65$, we have

$$I_l = 0.42\frac{\alpha}{C_f}\left(\frac{1}{8}\rho g\frac{H_b^2}{2}\cdot C_b \cdot \sin\alpha_b\cos\alpha_b\right). \tag{26}$$

The wave celerity at the breaking point is nearly equal to the wave group velocity, $(Cn)_b$, at that point, and the equation

$$H_b^2 = 2(H_{\mathrm{rms}})_b^2 \tag{27}$$

is valid (see Table 9.1 in *Goda* 1985a), where $(H_{\mathrm{rms}})_b$ is the root-mean-square height of irragular waves. Therefore, we can rewrite Eq. (26) as

$$I_l = 0.42\cdot\frac{\alpha}{C_f}\cdot P_l, \tag{28}$$

where

$$P_l = \frac{1}{8}\rho g(H_{\mathrm{rms}})_b^2(C_n)_b\sin\alpha_b\cos\alpha_b, \tag{29}$$

which is the longshore component of the wave energy flux per unit length of beach.

Komar and *Inman* (1970) investigated the longshore transport rate, based on the field data obtained by using the fluorescent sand tracer and proposed the equation

$$I_l = K\cdot P_l, \tag{30}$$

where K is the wave power cofficient. According to *Komar* and *Inman* (1970), K has a constant value of 0.77, whereas *Bailard* (1984) says that K is a function of the incident breaker and sediment characteristics, changing its value in the range from 0.11 to 1.15 in the field data.

From Eqs. (28) and (30), we have ultimately

$$\alpha = \frac{K}{0.42}\cdot C_f = (0.3\sim 2.7)\cdot C_f, \tag{31}$$

which means that the value of α is of the order of C_f, that is to say, being 0.01.

In the derivation up to Eq. (31), some implicit assumptions have been made for the significant wave height and the root-mean-square height. However, the final result is supported by the field evidences. The mean longshore advection speeds of sand and the mean longshore current velocities, which are the data quoted in *Komar* (1978), are plotted in Fig. 53, which gives the result of

$$\overline{V_s} = 0.01\cdot\overline{V_l}. \tag{32}$$

Equation (18) has been inferred through the above consideration, and is considered to reasonably explain the relation between the sand advection speed in the mean current direction and the mean current velocity as seen in Fig. 52.

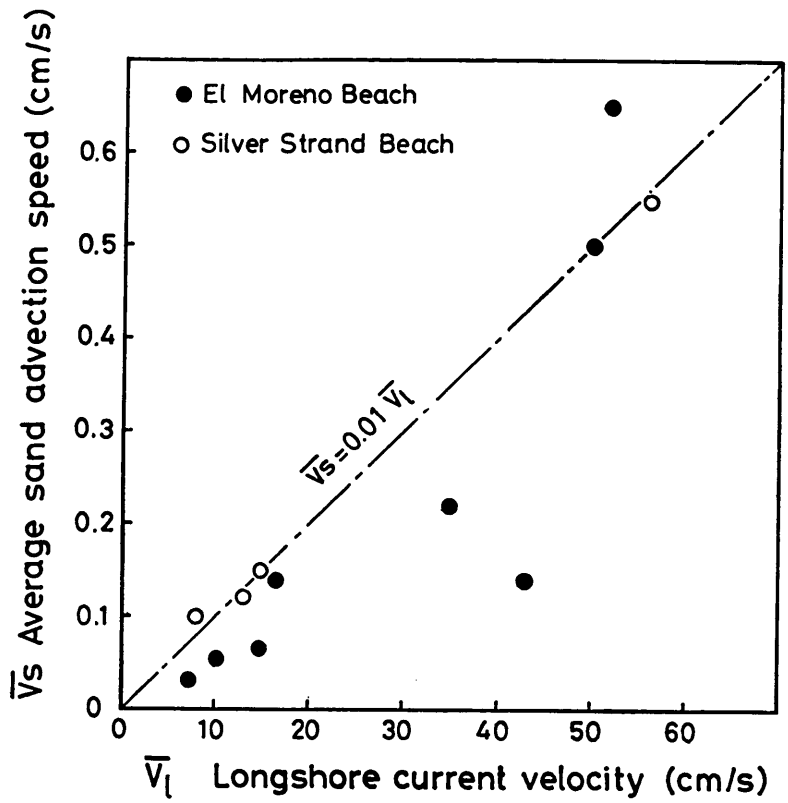

Fig.53 Longshore sand advection speed compared with longshore current velocities (measured by *Komar* 1978).

4.4 Advection Speed of Sand Movement in the Principal Wave Direction

Although the sand tracer is always moving to-and-fro in phase with the orbital velocity of waves, we are hare concerned only with the time averaged values of the tracer movement.

According to *Bowen* (1980) who applied the *Bagnold* model (1962, 1963) to the sediment transport in the sea, the instantaneous sediment transport formulae are

$$i_b=\frac{\varepsilon_b\cdot C_D\cdot\rho\cdot u^3}{\tan\phi-u\cdot\tan\beta/|u|}\ :\ \text{for bed load transport,} \tag{33}$$

$$i_s=\frac{\varepsilon_s\cdot C_D\cdot\rho\cdot u^3|u|}{w-u\cdot\tan\beta}\ :\ \text{for suspended load transport,} \tag{34}$$

where w is the fall velocity of the sediment, ε_b and ε_s are the bed load and suspended load efficiencies respectively, C_D is the drag coefficient, ρ is the water density, $\tan\phi$ is the frictional angle of the sediment and u is the total instantaneous velocity. *Bailard* (1981) employed these formulae with some modifications.

As easily inferred from the numerators in Eqs. (33) and (34), there are two important values of the third and fourth power of the total velocity for the bed load and the suspended load, respectively. Then, the contribution of the third velocity moment $\overline{U_p^3}$ to the advection speed will be examined at first. For this purpose, the values of skew-

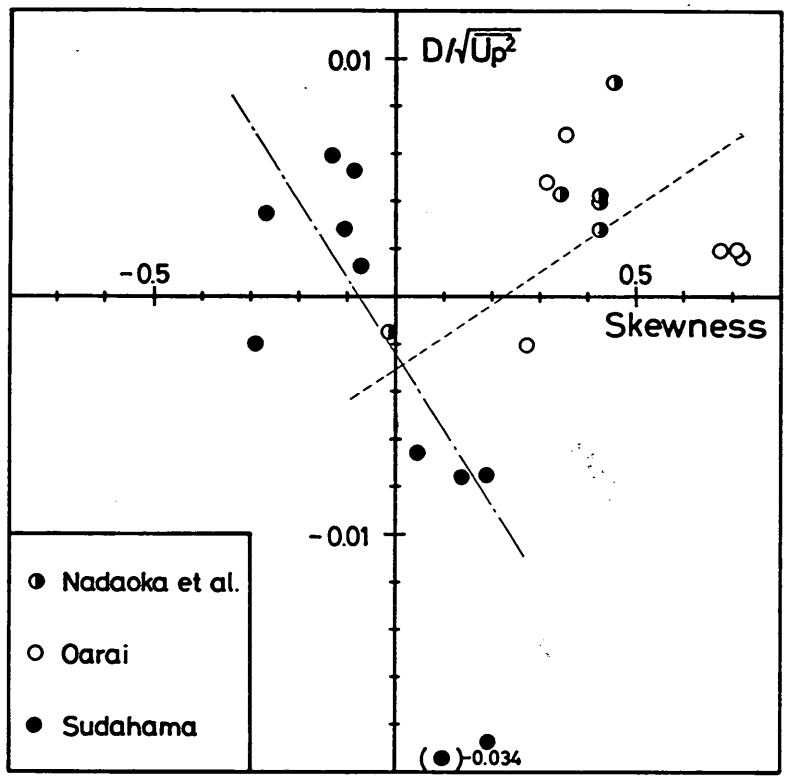

Fig.54 Dimensionless advection speed in the principal direction compared with the skewness.

ness for the velocity profile which are listed in the fifth column in Table 5 can be utilized, because the third velocity moment yields the skewness when it is divided by the third power of root-mean-square value $(\sqrt{\overline{U_p^2}})^3$ as shown by Eq. (6). The dimensionless advection speed $D/\sqrt{\overline{U_p^2}}$ is plotted against the skewness in Fig. 54. As seen in Fig. 54, there are two different tendencies. One is that the dimensionless advection speed decreases from positive to negative with the incerase of the value of skewness for data measured on Sudahama Beach, where the predominant long-period components of velocities existed. Another is that it increases with the skewness for the remaining data. As the dimensionless advection speed in the principal wave direction can be explained partially but not wholly by using only the skewness parameter, we need to take another parameter into account.

It might be said that the analysis in Fig. 54 has been done for one aspect of transport, i.e., bed load transport, although U_p is different from the total velocity u in Eqs. (33). Another aspect of sand transport, i. e., suspended load transport, has been formulated as Eq. (34), which has a term of the fourth velocity moment $\overline{U_p^3|U_p|}$. Therefore one may think that the fourth moment will provide a new parameter to explain the behavior of the dimensionless advection speed in Fig. 54. However, the value of $\overline{U_p^3|U_p|}$ will only exaggerate the value of $\overline{U_p^3}$, or skewness, and the two different tendencies observed in Fig.54 will not be brought into harmony by the introduction of this parameter.

Another approach for the explanation of the suspended load transport is thus nec-

essary. *Sternberg, Shi,* and *Dowing* (1984) continuously measured the concentration of suspended load by using the optical backscatter sensors in the surf zone. Based on the data obtained, they reported that the frequency and duration of individual suspension events were strongly correlated with incident wave conditions, and the events of suspensions were in phase with bores propagating across the surf zone. Therefore, it is better to use a parameter representing the characteristic of the bores which have distinct features of the forward tilting both in the surface profile and in the velocity profile. For this purpose, the velocity moments higher than the third power cannot be utilized, because their values are exaggerated versions of the skewness which is the parameter for indicating not the before-and-behind asymmetry but the up-and-down asymmetry in the velocity profile. This context can be easily understood when the process of data analysis is examined. The value of every velocity moment does not depend on the order of appearnce of digitized data, and it is unchanged by shuffing of the digitized data. On the other hand, the before-and-behind asymmetry is strongly dependent on the time sequence of profile data.

Goda (1985b) proposes a new parameter named the atiltness for the forward tilting of wave profile, which is defined by

$$\beta_3=\frac{1}{\left(\sqrt{\overline{(\dot{\eta})^2}}\right)^3}\cdot\overline{(\dot{\eta})^3}, \tag{35}$$

where η is the surface displacement from the mean sea level and the overdot in the expression denotes the differentiation with respect to time. Let us apply the concept of this parameter to the velocity profile. As seen in the concept figure of Fig. 55, the velocity profile of the forward tilting, when it is differentiated with respect to time, yields the up-and-down asymmetry in the acceleration profile, the magnitude of which can be evaluatd by the similar way as the skewness as follow :

$$\gamma_1=\overline{\dot{U}_p^3}. \tag{36}$$

When the velocity is differentiated with respect to time, the contribution of the longer period components to $\overline{\dot{U}_p^3}$ becomes smaller than that of shorter ones. As demonstrated in Fig.43, the long-period components of velocity fluctuations can cause a drift of

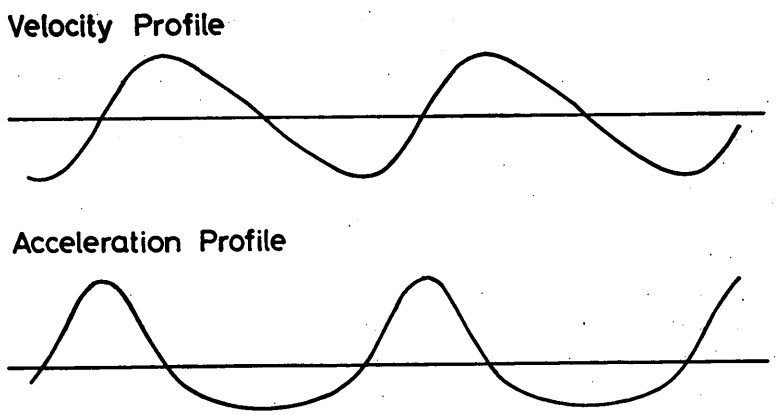

Fig.55 Velocity profile and corresponding acceleration profile.

the overall profile. The operation of differentiation can remove the effects of such long-period components, and the parameter defined by Eq. (36) mainly expresses the forward tilting of individual velocity fluctuations.

By using the newly defined parameter (Eq. 36), let us assume that the dimensionless advection speed in the principal direction can be approximately expressed as follow :

$$\frac{D}{\sqrt{\overline{U_p^2}}}=a\cdot\sqrt{\beta_1}+b\cdot\frac{\gamma_1}{g^3}, \tag{37}$$

where a and b are the coefficients and the second term in the right-hand side is normalized by dividing γ_1 with the third power of the acceleration of gravity.

The transport direction of suspended load should be taken care, because the newly defined parameter is considered to be related to the concentration of the suspended load alone. The suspended load generated at the passing of the bores will be easily transported by the subsequent orbital velocities in the directions of the latter until the suspended load comes to rest onto the sea bottom. In this process, the concentration of suspended load and its rate of transport are affected by both the previous situations and the instantaneous conditions. This phenomenon may be called the hysterisis effect on the suspended load, which is not included in Eq. (34) because of its dependency on the instantaneous velocities only. This is one more reason for not calculating the fourth moment.

As the subsequent orbital velocities change in both magnitudes and directions with respect to time, the net directions of suspended load transport may depend on the period of the orbital motion, or wave period T, and the time required by the suspended particle to fall some distance to the sea bottom. For example, in the case of large fall velocity of sand particles, the suspended load will be transported in the onshore direction by the onshore velocity just after the passing of the bores, because of its short settling time. On the other hand, in the case of small fall velocity it may be transported in the offshore direction by the subsequent offshore velocity.

According to the Shore Protection Manual, *Coastal Engineering Research Center* (1977), the direction of suspended load transport in the surf zone can be approximately explained by using a dimensionless fall-time parameter

$$F_0=H_0/(w\cdot T), \tag{38}$$

where H_0 is the deep water wave height, T is the wave period and w is the fall velocity of the beach sediment. Equation (38) represents a ratio of the time required by the particle to fall over a distance about equal to the maximum depth in the surf zone, H_0/w, to the time available between two arriving wave crests, T. The data plotted in the Shore Protection Manual suggest that when the values of F_0 are greater than 1, that is to say $H_0/w > T$, the significant concentration of suspended load are expected to diffuse offshore and deposit in the offshore side.

In the cases of the observations reported here, the mean diameters of bed material are ranged from 0.16mm to 0.24mm (see Tabe 1), which correspond to the fall velocity of about 1.8 cm/s to 3.2 cm/s. If the period of incident waves, about 8 seconds (see Table 1), is taken for T, the value of a denominator in Eq. (38) becomes about 14 to 25 cm. By referring to the value of H_0 in Table 1, we estimate the values of F_0 being qreater than 1. Therefore, the suspended load is thought to be transported in the offshore direction.

The above consideration is applicable for the velocity fields due to the incident waves alone, but it is not so for the case in which the predominant long-period compo-

nents coexist. In the latter case, the direction of the combined velocity depends almost on that of the long-period components. As seen in Fig. 43, for example, when the long-period velocity components have a large positive value, the velocity combined with those of incident waves fluctuate mainly in the positive side. Under these conditions, a practice of taking the period of the incident waves as T in Eq. (38) is not appropriate, because the suspended load dut to the passing of bores will be transported in the direction of the velocity of long-period components.

The direction of the net suspended load transport in the velocity fields containing the predominant long-period components will be inferred as follows. The values of skewness for the long-period velocity components are negative as explained in Section 3.3, which means that the total duration of the time when the direction of velocity is onshore is longer than that of offshore. The high concentration of suspended load occurs when the bores pass through. If the time interval between two arriving bores is constant, the frequency of the bores passing through a fixed point becomes larger during the time periods of onshore velocities than those of offshore ones, because the duration of the former is longer than that of the latter. This situation can be recognized in Fig. 43. Therefore, the larger amount of sand is transported to the onshore direction in suspension, which yields the net onshore transport.

The discussions on the direction of suspended load transport are summarized into the following two points :

(a) When the velocity field is mainly due to the incident waves, the suspended load diffuses offshore and deposits; the value of coefficient b in Eq. (37) is negative.

(b) When there coexist the predominant long-period components, the net suspended losd is in the onshore direction; the value of b is positive.

Therefore the sign of the coefficint b should be changed based on whether the predominant long-period components coexist or not with the incident waves. For this purpose, the values of skewness or $\overline{U_p^3}$ can be utilized as a first step, because it is positive when the incident wave components are relatively large in the case of (a) and is negative when the long-period components are relatively large in the case of (b) as previously mentioned in Section 3.3. Thus, Eq. (37) is rewitten as

$$\frac{D}{\sqrt{\overline{U_p^2}}}=a\cdot\sqrt{\beta_1}+b\cdot\mathrm{sgn}(\sqrt{\beta_1})\cdot\frac{\gamma_1}{g^3}, \tag{39}$$

where $\mathrm{sgn}(\sqrt{\beta_1})$ takes the value of $+1$ or -1 depending on whether the skewness is positive or negative, and the value of redefined coefficient b should be a negative.

The value of γ_1 defined by Eq. (36) can be obtained by multiplying the third power of $\sqrt{\overline{\dot{U}_p^2}}$ by the skewness of the acceleration profile which are listed in Table 5. Using a regression analysis for Eq. (39) with the data listed in Table 5, we get the values of 0.024 and -85.1 for a and b, respectively. In turn, the value of the quantity in the right-hand side of Eq. (39) for each sand tracer has been calculated with the values of coefficients obtained, and it is plotted on the abscissa with the corresponding dimensionless advection speed on the ordinate in Fig. 56.

Two different tendencies observed in Fig. 54 have disappeared in Fig. 56. Except three data points, the data are gathered around a straight line having the inclination of 0.85. The straight line is decided by applying the least squares method to the data excluding the three distant points so that the line should pass through the origin. By multiplying the coefficients a and b with the value of 0.85 we have the following relation :

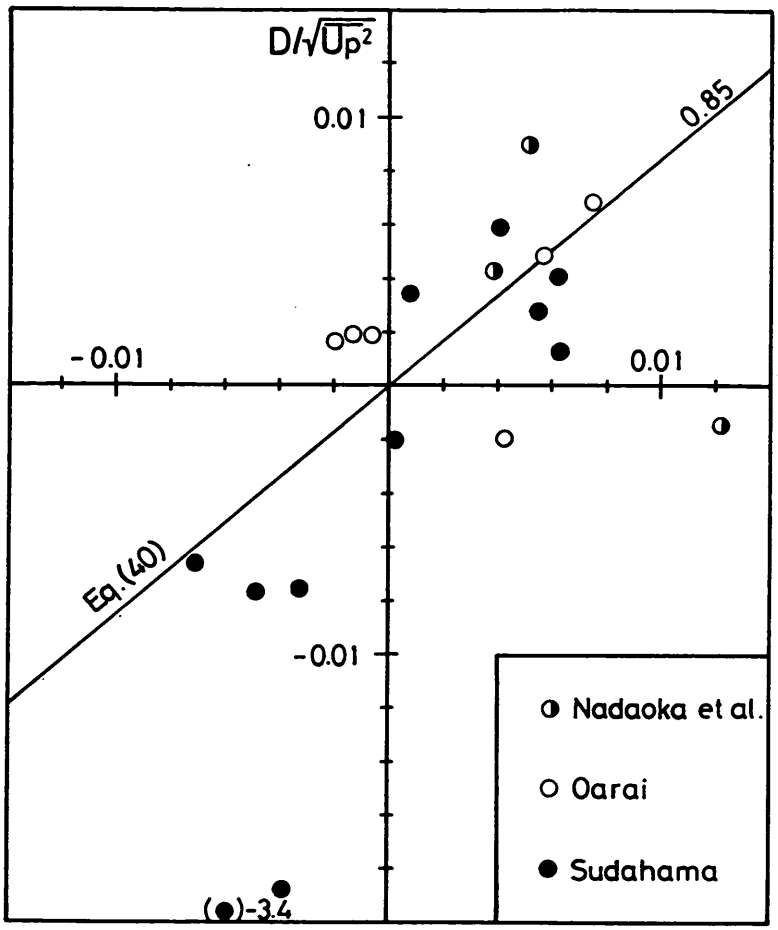

Fig.56 Dimensionless advection speed in the principal direction compared with the skewness and the magnitudes of forward inclination of velocity profiles. (The abscissa is the right-hand side of Eq.39 with $a=0.024$ and $b=-85.1$.)

$$\frac{D}{\sqrt{\overline{U_p^2}}}=0.02\cdot\sqrt{\beta_1}-72.4\cdot\mathrm{sgn}(\sqrt{\beta_1})\frac{\overline{\dot{U}_p^3}}{g^3}. \tag{40}$$

As previously explained, the first term in the right-hand side of Eq. (40) is considered to correspond to the bed load transport, while the second one to the suspended load transport. Equation (40) indicates that the directions of bed and suspended load transports are opposite each other, because $\overline{\dot{U}_p^3}$ usually takes a positive value.

4.5 Mixing Depth of Sand Tracer

As to the mixing depth of sand tracer, five definitions have been compared by *Kraus* (1985) using the data of vertical distribution of fluorescent sand tracer on the beaches. He concluded that the procedure defining the mixing depth as that depth containig 80

% of the total tracer in a core sample is the most preferable method. In this report the mixing depth b is defined in the same manner as *Kraus* (1985) and the calculated results are listed in Table 3.

Sunamura and *Kraus* (1985) presented the shear stress model to predict the average depth of wave-induced sediment mixing in the surf zone. The model shows that the mixing depth normalized with the sediment grain diameter is linearly related to the Shields parameter,

$$\bar{b}/d_m = K_1 \cdot \Psi_b, \tag{41}$$

$$\Psi_b = \frac{1}{2} \cdot \frac{f_w U_b^2}{(\rho_s/\rho - 1) g d_m}, \tag{42}$$

where Ψ_b is the Shields parameter defined with maximum near-bottom horizontal orbital velocity of the breaking waves U_b, K_1 is a coefficient, f_w is a wave friction factor and an overbar above b denotes the average value in the surf zone.

Equations (41) and (42) suggest that the averaged mixing depth b is proportional to the square of the velocity of the breaking waves. Then, let us examine whether this relation can be applied to the local mixing depth and the local velocities or not. The mixing depths listed in Table 3 are plotted against the mean-square values of velocities divided by the gravity of acceleration, $\overline{U_p^2}/g$, in Fig.57. Although some scatter is observed in the data points, the straight line drawn through the origin gives the result of

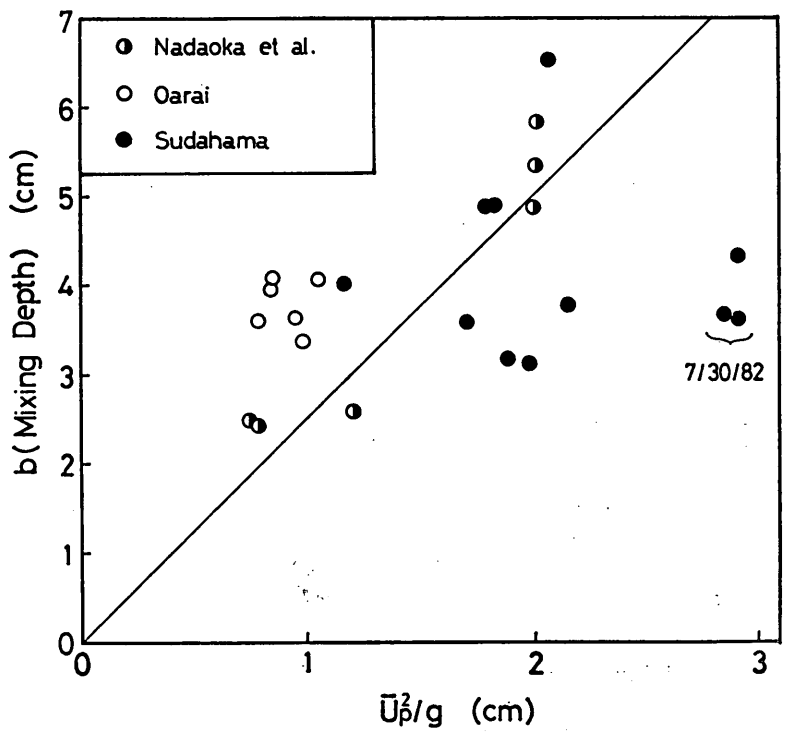

Fig.57 Local mixing depth as a function of the mean-square of velocities.

$$b=2.5\cdot\overline{U_p^2}/g. \tag{43}$$

Equation (43) can be rewritten with the local wave height by using the following assumptions. Let us assume that the significant amplitude of velocity fluctuation $(H_{up})_{1/3}/2$ is evaluated by the equation

$$(H_{up})_{1/3}=4.0\cdot\sqrt{\overline{U_p^2}}. \tag{44}$$

On the basis of the shallow-water approximation, the following equation is assumed valid :

$$\frac{(H_{up})_{1/3}}{2}=\frac{1}{2}\cdot\frac{H_{1/3}}{h}\sqrt{gh}=\frac{1}{2}\sqrt{\gamma gH_{1/3}}, \tag{45}$$

even if the predominant long-period components coexist. In the above, $H_{1/3}$ and h are the local significant wave height and the water depth, respectively, and γ is the ratio of $H_{1/3}$ to h, being approximately equal to 0.6-0.65 in the case of the irregular waves (see *Goda* 1985a). By substituting Eqs. (44) and (45) into Eq. (43), we have

$$b\fallingdotseq 0.156\cdot\gamma\cdot H_{1/3}=0.10\cdot H_{1/3}. \tag{46}$$

Furthermore, the average mixing depth in the surf zone can be estimated by the equation

$$\overline{b}=\frac{1}{X_b}\int_0^{X_b} b\,dx, \tag{47}$$

where X_b is the width of the surf zone. By asumming a constant sloping beach, $h=x\tan\beta$, and γ being constant in the surf zone, we can integrate Eq. (47) as follow :

$$\overline{b}=\frac{1}{X_b}\int_0^{X_b} 0.10\cdot\gamma\cdot x\tan\beta\cdot dx=0.05\cdot H_b, \tag{48}$$

where H_b is the significant wave height at the wave breaking point.

Sunamura and *Kraus* (1985), starting from Eq. (41), empirically obtained a linear dependence of $\overline{b}$ on H_b as follow :

$$\overline{b}=0.027\cdot H_b. \tag{49}$$

The values of coefficient in Eqs. (48) and (49) are of the same order, but the former is about twice as large as the latter. Some causes are pointed out for the difference between these coefficients. First, the mean current velocity, which varies according to local beach conditions, has not been included in both considerations. Second, the data obtained by *Kraus* (1985) showed that the onshore-offshore distributions of the mixing depth were different in case by case ; they were nearly constant in some cases, but they were increasing or decreasing in the offshore direction in other cases. In opposite to these field evidences, Eq. (48) is based on the linear distribution of mixing depth increasing with the water depth; it is zero at the shoreline and maximum at the wave breaking point. The appropriateness of Eq. (48) entirely depends on the assumptions regarding the wave field in the surf zone, which may not have been correct. Under the present situation, however, it is not possible to clarify the cause of the difference between Eqs. (48) and (49). At least in this report, the mixing depth should be expressed in terms of the velocity fluctuations as in Eq. (43), because the local wave height have not been measured in our observations.

4.6 Local Sand Transport Rate

In much the same way as the bulk volume of longshore sand transport rate (Eq.19), a bulk volume of local sand transport rate per unit width Q_t is given by the equation

$$Q_t = b \cdot V_t. \tag{50}$$

The local advection velocity of the sediment V_t has been decomposed into the two components V_s and D in the directions of mean currents and the incident waves, respectively. These components can be approximately evaluated by means of Eqs. (18) and (40). The local sand transport rate is also decomposed into such two directions as follows:

$$Q_s = b \cdot V_s, \tag{51}$$

$$Q_D = b \cdot D. \tag{52}$$

The mixing depth of the bottom sediment b in Eq. (50) can be estimated by using Eq. (43).

By substituting Eqs. (18), (40) and (43) into Eqs. (51) and (52) respectively, we have

$$Q_s = \frac{0.025}{g} \cdot \overline{U_p^2} \cdot \overline{V}, \tag{53}$$

$$\begin{aligned} Q_D &= [0.02\sqrt{\beta_1}\sqrt{\overline{U_p^2}}] \cdot b - \left[72.4 \cdot \mathrm{sgn}(\sqrt{\beta_1}) \frac{\overline{\dot{U}_p^3}}{g^3} \sqrt{\overline{U_p^2}}\right] \cdot b \\ &= \frac{1}{g}\left[0.05 \cdot \overline{U_p^3} - 181 \cdot \mathrm{sgn}(\overline{U_p^3}) \cdot (\overline{U_p^2})^{3/2} \cdot \frac{\overline{\dot{U}_p^3}}{g^3}\right]. \end{aligned} \tag{54}$$

The first term in the right-hand side of Eq. (54) mainly corresponds to the bed load transport, while the second one to the suspended load transport as previously explained in Section 4.4. The sand transport in the mean current direction occurs simultaneously in these two different transport modes. However, the sand transport rate in that direction is expressed by only one term in Eq. (53). This is because it is almost impossible to separate the sand transport rate in the mean current direction into the above two modes, and Eq. (53) provides an empirical relation inclusive of suspended load transport.

Based on Eq. (54), further interesting discussions can be made. The mixing depth b is multiplied by the second term in the right-hand side of Eq. (40) to yield the contribution of suspended load to the total sand transport rate in Eq. (54). This operation looks strange because the mixing process is a phenomenon in the sea bottom, whereas the suspension of the bed material is that above the sea bottom. This apparent strangeness, however, may serve to understand the mechanics of sand transport in suspension in the surf zone.

For simplicity, let us pay our attention to one sand particle which has the same diameter as the others. The particle pausing on the sea bottom surface at first is suspended when the bore passes over it. Subsequently it is transported in suspension to some distance with the same velocity as the fluid one and deposits after several seconds on the sea bottom. Next, it is buried into the sea bottom due to the some mixing process of bed material. Then it losses an opportunity to be suspended again for a while. The time required for the particle to emerge again on the sea bottom surface

becomes longer with increase in the mixing depth of the bed material. The elongation of the reappearance time reduces the apparent advection speed. This effect is already contained in the empirically obtained advection speed D (the second term of the right-hand side of Eq. 40). While it is being buried in the sea bottom, the other particles which have been buried in the sea bottom to some depth initially at that point are successively suspended and transported to other points, of course with the same apparent advection speed as that of the particle we pay our attention to. The number of these particles suspended, or bulk volume of the particles, becomes large with increase in the reappearing time of our particle which is inferred to depend on the mixing depth b. Therefore, in order to obtain the total bulk volume of sand transport rate in suspension, the mixing depth b should be multiplied by the advection speed such as the second term in the right-hand side of Eq. (54).

Discussions have actively been held concerning whether the suspended load or the bed load transport is more important in the surf zone. For examples, *Komar* (1978) concluded that the suspended load is much less significant than the bed load transport, while *Sternberg*, *Shi* and *Downing* (1984) reported that all of the longshore transport at Leadbetter beach could be accounted for by the suspended load transport. We shall also examine the above problem by using Eq. (54). Let q_b and q_s be the absolute values of bed load and suspended load transport rates in the principal wave direction, respectively. They can be expressed from Eq. (54) as follows :

$$q_b = \left| \frac{0.05 \cdot \overline{U_p^3}}{g} \right| , \tag{55}$$

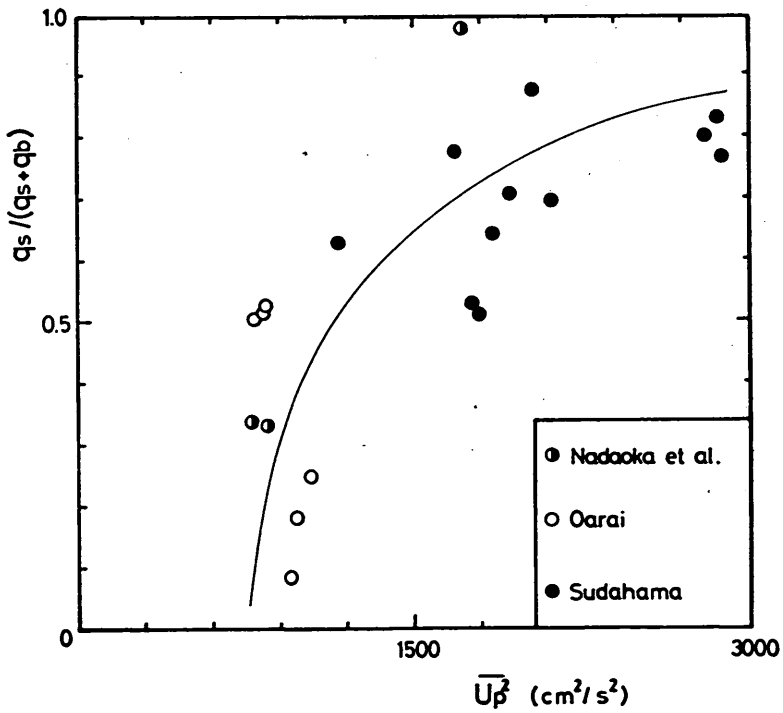

Fig.58 Rate of suspended load transport compared mith mean-square of velocities in the principal wave direction.

$$q_s = \left| \frac{181 \cdot (\overline{U_p^2})^{3/2} \cdot \overline{\dot{U}_p^3}}{g^4} \right| , \qquad (56)$$

where sgn $(\overline{U_p^3})$ is neglected because it has the absolute value of unity. Utilizing the values listed in Table 5, we can calculate the values of $q_s/(q_s+q_b)$ on the basis of Eqs. (55) and (56). The obtained values of $q_s/(q_s+q_b)$ are plotted on the ordinate against the mean-square values of the velocities in the principal wave direction $\overline{U_p^2}$ on the abscissa in Fig. 58. According to Fig. 58, the ratio of the absolute suspended load transport to the total transport varies among the value of less than 0.1 to nearly 1.0 with a tendency of increase with the mean-square value of the velocity in the principal wave direction. From this tendency of increase, it can be inferred that the suspended load transport will become more significant under the high wave conditions.

5. Summary

In order to study the local sand movements in the surf zone, the fluorescent sand tracer has been injected at the center of a circle. After that, the core samples have been taken from the sixteen points on the time intervals of fifteen minutes for about five hours. At the same time, the horizontal two components of fluid velocities have been measured at the injection point by using the electromagnetic currentmeter. The field observations have been carried out five times on three beaches facing to the Pacific Ocean. In this report, the relations between the local sand movements and the fluid dynamics have been examined on the basis of the data obtained. The major conclusions in this report are as follows :

(1) In some cases, the values of skewness for the velocity component in the principal wave directions, in which the predominant long-period fluctuations coexist, are negative. The data analyses show that the values of skewness for the incident wave components are positive, while those for the long-period one are negative which make the values of skewness for the velocities combined of these two components to be negative.

(2) The advection speed of sand tracer in the mean current direction is about 1% of the mean current velocity (Eq. 18). This relation is supported by a semi-theoretical analysis using the formulae of longshore current velocity and the longshore sand transport rate.

(3) The advection speed of sand tracer in the principal wave direction depends on not only the up-and-down asymmetry but also the before-and-behind asymmetry in the velocity profiles (Eq. 40). The former asymmetry is considered to be related to the bed load transport and the latter one to the suspended load transport. The magnitude of the before-and-behind asymmetry is evaluated by calculating the skewness for the acceleration profiles.

(4) The local mixing depth of the bed material is approximately proportional to the mean-square value of fluid velocities (Eq. 43), which suggests the linear relationship with the local wave height.

(5) For the first approximation, the equations for the local sand transport rate are proposed (Eq. 54) which are restricted to the field conditions under which the observations have been carried out.

(6) Based on the equation of local sand transport rate, the transporting conditions of suspended load are inferred so that the bed material may be transmittently transported in suspension in relatively short durations and be buried in the sea bottom due to the process of mixing of bed material during the remaining periods.

(7) The ratio of the absolute suspended load transport to the sum of the absolute

transports of the suspended and the bed load becomes large with increase in the mean-square values of velocities, which suggests that the suspended load transport will become more significant under the high wave conditions.

The local sand transport rate equations empirically obtained in this study are not necessarily enough, because the local bottom slope, sediment characteristics, the critical velocity of the onset of sand movement and other factors are not taken into account and the assumption in the form of Eq. (39) is for the first approximation. Furthermore, it is a question whether the fluid velocities at the point of about 20 cm above the sea bottom is appropriate or not to be related with the sand transport rate. It is, however, clear for the locol sand transport in the onshore-offshore direction that both the up-and down and the before-and-behind asymmetry in the velocity profiles are important factors. Unfortunately, these distinct features in the velocity profiles cannot be predicted by the numerical simulations at present. Therefore, we also should investigate the relations between the non-lineality of waves in the surf zone and representative values of deep water waves in the field as *Bailard* (1982) has been doing. Emphasis should be placed on the formation of the before-and-behind asymmetry in the velocity profiles during the wave shoaling process and on its quantitative formulation within the surf zone. Finally, the results obtained by using the fluorescent sand tracer should be cross-checked with the results of wholly different observation methods. For this purpose, the continuous measurements of the suspended transport by utilizing the HORF, Hazaki Oceanogrphical Research Facility-Photo. 5, in the storm wave conditions are being planned (*Irie*, *Terasaki* and *Katoh 1985*).

(*Received on Sept. 30, 1985*)

Acknowledgements

The authors are grateful to Dr. Yoshimi Goda, the Deputy Director General of the Port and Harbour Research Institute, for helpful suggestions especially about his new parameter of the forward tilting in wave profiles and his critical reading of the manuscript. The authors also should like to express their heartfelt thanks to Mr. Kazuo Nadaoka, Tokyo Institute of Technology, for his great contributions on the field observations and his concepts shown in the first report when he was a member of the Littoral Drift Laboratory, the Port and Harbour Research Institute. The authors received earnest cooperation from Mr. Isao Irie, Chief of the Littoral Drift Laboratory, and Mr. Yoshiaki Kuriyama, Member of the Littoral Drift Laboratory, concerning the field observations in 1983.

References

1) BAGNOLD, R. A. (1962): Autosuspension of transported sediment; Turbidity currents, *Proc. of the Royal Socity of London, Series A*, Vol. 265, pp. 315-319.
2) BAGNOLD, R. A. (1963): Mechanics of marine sedimentation, *in the Sea*, Vol. 3, Edited by M. H. Hill, Intersience, pp. 507-528.
3) BAILARD, J. A. (1981): An energetics total load sediment transport model for a plane sloping beach, *J. Geophy. Res.*, Vol. 86, No.C11, pp. 10938-10954.
4) BAILARD, J. A. (1982): Modeling on-offshore sediment transport in the surf zone, *Proc. 18th Int. Conf. on Coastal Eng.*, pp. 1419-1438.
5) BAILARD, J. A. (1984): A simplified model for longshore sediment transport, *Proc. 19th Int. Conf. On Coastal Eng.*, pp. 1454-1470.
6) BOWEN, A. J. (1980): Simple models of nearshore sedimentation; Beach profile and longshore bars, *in the coastling of Canada*, Edited by McCann, S. B., Geological Survey of

Canada, Ottawa, pp. 1-11.
7) Coastal Engineering Research Center, U. S. Army (1977): Shore protection manual, *U. S. Government Printing Office*, Vol. 1, pp. 4-81 to 4-84.
8) GODA, Y. (1985a): Random seas and design of maritime structures, *University of Tokyo Press*, 323p.
9) GODA, Y. (1985b): Numericale examination of several statistical parameters of sea waves, *Report of the Port and Harbour Research Institute*, Ministry of Transport, Japan, Vol. 24, No. 4 (in Japanese).
10) GUZA, R. T. and E. B. Thornton (1982): Swash oscillations on a natural beach, *J. Geophy. Res.*, Vol. 87, No.C1, pp. 483-491.
11) HASHIMOTO, H. and T. Uda (1982): Field investigation of beach profile changes and the analysis using empirical eigenfunctions, *Proc. 18th Int. Conf. on Coastal Eng.*, pp. 1369-1384.
12) HATTORI, M. (1982): Field study on onshore-offshore sediment transport, *Proc. 18th Int. Conf. on Coastal Eng.*, pp. 923-940.
13) HOLMAN, R. A., D. A. HUNTLEY and A. J. BOWEN (1978): Infragravity waves in storm conditions, *Proc. 16th Int. Conf. on Coastal Eng.*, pp. 268-284.
14) HOTTA, S., M. MIZUGUCHI and M. ISOBE (1981): Observations of long period waves in the nearshore zone, *Coastal Eng. in Japan*, Vol. 24, pp. 41-76.
15) HOTTA, S., M. MIZUGUCHI. and M. ISOBE (1982): A field Study of waves in the nearshore zone, *Proc. 18th Int. Conf. on Coastal Eng.*, pp. 38-57.
16) HUNTLEY, D. A. and A. J. BOWEN (1973): Field observation of edge waves, *Nature*, Vol. 243, No. 5403, pp. 160-162.
17) HUNTLEY, D. A. (1976): Long-period waves on a natural beach, *J. Geophy. Res.*, Vol. 81, No.36, pp.6441-6449.
18) HUNTLEY, D. A. and A. J. BOWEN (1978): Beach cusps and edge waves, *Proc. 16th Int. Conf. on Coastal Eng.*, pp. 1378-1393.
19) HUNTLEY, D. A., R. T. GUZA and E. B. THORNTON (1981): Field observations of surf beats. 1. Progressive edge waves, *J. Geophy. Res.*, Vol. 86, No. C7, pp.6451-6466.
20) IRIE, I., K. TERASAKI and K. KATOH (1985): Laboratory study on the observation methods of sediment transport as focussed on suspension of sediment above sand ripples, *Report of the port and Harbour Research Institute*, Ministry of Transport, Japan, Vol. 24, No.2, pp. 123-156 (in Japanese).
21) KATOK, K. (1981): Analysis of edge waves by means of empirical eigenfunction, *Report of the Port and Harbour Research Institute*, Ministry of Transport, Japan, Vol. 20, No. 3, pp.3-51.
22) KATOH, K., N. TANAKA and I. IRIE (1984): Field observation on suspended-load in the surf zone, *Proc. 19th Int. Conf. on Coastal Eng.*, pp. 1846-1862.
23) KOMAR, P. D. and D. L. INMAN (1970): Longshore sand transport on beaches, *J. Geophy. Res.*, Vol. 75, No. 30, pp. 5914-5927.
24) KOMAR. P.D. (1978): Relative quantities of suspension versus bed-load transport on beaches, J. of Sedimentary Petrology, Vol. 48, pp. 921-932.
25) KRAUS, N. C., H. HANSEN and S. HARIKAI (1984): Shoreline change at Oarai Beach: Past, present and future, *Proc. 19th Int. Conf. on Coastal Eng.*, pp. 2107-2123.
26) KRAUS, N. C. (1985): Field observations on vertical mixing of sand in the surf zone, *Jour. of Sedimentary Petrology*, Vol. 55, No. 1, pp. 3-14.
27) LONGUET-HIGGINS, M. S. (1970): Longshore currents generated by obliquely incident sea waves, 1 and 2, *J.Geophy. Res.*, Vol.75, No. 33, pp. 6778-6789, and pp. 6790-6801.
28) MIZUGUCHI, M. (1982): Individual wave analysis of irregular wave deformation in the nearshore zone, *Proc. 18th Int. Conf. on Coastal Eng.*, pp. 485-504.
29) NADAOKA, K., N. TANAKA and K. KATOH (1981): Field observation of local sand movements in the surf zone using fluorescent sand tracer, *Report of the Port and Harbour Research Institute*, Ministry of Transport, Japan, Vol. 20, No. 2, pp. 75-126 (in Japanese).
30) NAGATA, Y. (1964): The statistical properties of orbital wave motions and their applica-

tions for the measurement of directional wave spectra, *Jour. of Oceanographical Soc. of Japan*, Vol. 19, No. 4, pp. 169-181.

31) SASAKI, T. and K. HORIKAWA (1975): Nearshore current system on a gently sloping bottom, *Coastal Eng. in Japan*, Vol. 18, pp. 123-142.

32) SASAKI, T.and K. HORIKAWA (1978): Observation of nearshore current and edge waves, *Proc. 16th Int. Conf. on Coastal Eng.*, pp. 791-809.

33) STERNBERG, R. W., N. C. SHI and J. P. DOWING (1984): Field investigations of suspended transport in the nearshore zone, *Proc. 19th Int. Conf. on Coastal Eng.*, pp. 1782-1798.

34) SUHAYDA, J. N. (1974): Standing waves on beaches, *J. Geophy. Res.*, Vol. 79, No. 21, pp. 3065-3071.

35) SUNAMURA, T. and N. C. KRAUS (1985): Prediction of average mixing depth of sediment in the surf zone, *Marine Geology*, 62, pp. 1-12.